THE EXAMINATION OF OIP5 EXPRESSION IN RENAL CELL CARCINOMA (RCC) AND DURING RCC PROGRESSION

THE EXAMINATION OF OIP5 EXPRESSION IN RENAL CELL CARCINOMA (RCC) AND DURING RCC PROGRESSION

By

MATHILDA CHOW, B.Sc. Honours

A Thesis

Submitted to the School of Graduate Studies

In Partial Fulfillment of the Requirements

For the Degree

Master of Science

McMaster University

MASTER OF SCIENCE (2020)

McMaster University, Hamilton, Ontario

Faculty of Health Sciences, Medical Sciences Graduate Program- Cancer and Genetics

TITLE: The Examination of OIP5 Expression in Renal Cell Carcinoma (RCC) and during RCC progression

AUTHUOR: Mathilda Chow, B.Sc. (McMaster University)

SUPERVISOR: Dr. Damu Tang

SUPERVISORY COMMITTEE: Dr. Peter Whyte

Dr. Anil Kapoor

NUMBER OF PAGES: xiv, 72

LAY ABSTRACT

Renal Cell Carcinoma (RCC) is the most lethal kidney cancer and accounts for approximate 2%-3% adult malignant neoplasm. The assessment of RCC prognosis and the subsequent treatments are depending on the exclusive clinical criteria, therefore, it is necessary to explore promising biomarkers and therapeutic targets to improve risk assessment and treatment. OIP5 is a relative new protein and its expression was increased in several cancers including clear cell RCC (ccRCC). However, its expression in papillary RCC (pRCC) and its impacts on RCC remain unclear. Therefore, this study is aimed to investigate the role of OIP5 in RCC and during RCC progression. The results suggested that OIP5 enhances the growth, proliferation, and invasion of pRCC cells. Furthermore, by using mouse model of pRCC, OIP5 was found to promote tumorigenesis. In patients, advanced ccRCC and pRCC tumors expressed significantly higher levels of OIP5, and these patients are associated with poor overall survival. From our animal RCC research, we discovered that tumors with increased OIP5 also expressed higher levels of a protein called PLK1; this protein is known to promote cell proliferation. In this context, a PLK1 inhibitor can inhibit the proliferation of pRCC cells expresses high levels of OIP5, suggesting that advanced pRCC with OIP5 expression increased can be treated with PLK1 inhibitor. This possibility should be investigated in future. Should this be confirmed, it will offer the first effective therapy for patients with advanced pRCCs harboring elevated OIP5 expression.

ABSTRACT

Renal Cell Carcinoma (RCC) is the most lethal kidney cancer and accounts for approximate 2%-3% adult malignant neoplasm. The current risk assessment on which treatment decisions are formulated largely relies on clinical criteria. Improvement in predicting prognosis requires the use of molecular events or biomarkers. OIP5 (Mis18β) is accumulated in telophase-G1 centromere and plays a critical role in centromere formation. Mis18β forms Mis18 heterotetramer with Mis18α and the complex is involved in the deposition of new centromeric protein A (CENP-A) nucleosomes, which is essential for centromere/kinetochore structure and functions. In normal individual, OIP5 is intensively expressed in testis, while recent studies have demonstrated that OIP5 promotes the initiation and progression of several cancers. However, its function in RCC remains unclear. This thesis thus aims to examine the hypothesis that OIP5 plays in RCC pathogenesis. *In vitro* studies demonstrated that overexpression of OIP5 promoted cell growth, proliferation, and invasion in ACHN pRCC cells. In comparison to ACHN cells stably expressing an empty vector (EV), ACHN OIP5 cells produced xenografts with a significantly enhanced ability with concurrent upregulation of PLK1 and other factors that are likely contribute to cell cycle progression. PLK1 plays important roles in promoting M phase progression, which is in accordance with an important role of OIP5 in centromere formation. Importantly, the PLK1 inhibitor BI2536 led to significantly more cells arrested in M phase compared to OIP5 EV cells, implying a reliance of PLK1 function to drive ACHN OIP5 cells progression through M phase. This property suggests an appealing scenario to treat pRCCs with OIP5 upregulation. Intriguingly, this possibility is supported by our clinical investigation. In our analysis of OIP5 expression in primary RCC (n=57), OIP5 upregulation was found

in both ccRCC and pRCC tumors compared to their adjacent non-tumor tissues. The upregulation is associated with ccRCC and pRCC progression as well as prognosis. Both ccRCC and pRCC tumors with elevated OIP5 expression are correlated with poor overall survival compared to those without the upregulation. Collectively, this thesis reveals a novel and important contribution of OIP5 in RCC, particularly pRCC; targeting PLK1 might be an option in treating pRCCs expressing high levels of OIP5.

ACKNOWLEDGEMENTS

First, and most importantly , I would like to express my deepest appreciation to my supervisor Dr. Damu Tang. Thank you so much for providing me the opportunity to be your graduate student for the past two years, as well as your undergraduate thesis student and research technician. This thesis would not have been possible without your crucial help, support and patience. I am greatly inspired and impressed by your enthusiasm, motivation and persistence toward to research. I have more thanks for you than I have room to write, and I will be forever grateful for all of your guidance. The years I spent in your lab will always be a wonderful, enlightening, and rewarding experience of my life.

I would like to thank my committee members, Dr. Peter Whyte and Dr. Anil Kapoor for the insights and suggestions on my project, as well as taking time out to attend my committee meetings from their busy schedule.

To Dr. Wenjuan Mei, Dr. Yanzhi Jiang, and Dr-soon-to-be. Yan Gu, without whom I would not be able to complete my thesis, thank you so much for being such great mentors throughout the time. I truly appreciated your invaluable help and support. You have not only taught me the lab techniques, but also have shown me what it means to be passionate on what you do. Our countless lunch, dinners and coffee really cheered me up. I would also like to thank the rest of former and current members in Tang lab- Dr. Diane Ojo, Dr. Nicholas Wang, Dr. Xiaozeng Lin, David Rodriguez, Marc Ramkairsingh, Kuncheng Zhao, Sherry Peng, and Riad Houha for their continuous support and help.

I would like to express my deepest gratitude to my parents. I would never be where I am without your constant support and encouragement. Thank you so much for always being there for me.

To my best friend, Cassandra, your support and encouragement worth more than I can express on paper. Thank you for being a such sincere friend, assignment partner, proofreader and animal room buddy. I am so grateful to have you as my friend since the first day of my university life. We went through every high's and low's in the past seven years. I will miss all of the moments we spent together.

To my boyfriend, Edward, thank you so much for being so supportive while I was working on my thesis. Thank you for the late-night pick-ups, for being understanding, and for being such a great friend.

To Karbi and Yeti, my cats. I feel so blessed that I can have you two as my company. Thank you for being my emotional support.

TABLE OF CONTENTS

LIST OF TABLES

I. INTRODUCTION

IV. RESULTS

LIST OF FIGURES

I. INTRODUCTION

IV. RESULTS

LIST OF ABBREVIATIONS

Akt	Protein kinase B
APC/C	Anaphase promoting complex/cyclosome
AT	Adjacent tissue
AURKB	Aurora B kinase
BUB1	Mitotic checkpoint serine/threonine-protein kinase
CCNB2	Cyclin B2
ccRCC	Clear cell renal cell carcinoma
CED/CHR	cycle-dependent element/cell cycle genes homology region
CDK	cyclin dependent kinase
CENP-A	Centromere-specific histone H3 variant
chRCC	Chromophobe renal cell carcinoma
DNA-PK	DNA-dependent protein kinase
EMT	epithelial-mesenchymal transition
ERK1/2	Extracellular signal regulated kinase 1 and 2
EV	Empty vector
FBS	Fetal bovine serum
GSK-3β	Glycogen synthase kinase 3 beta

HIF	hypoxia-inducible factor
HJURP	Holliday junction recognition protein
IHC	Immunohistochemistry
ILK	integrin-linked kinase
MAPK	Mitogen activated protein kinase
MAP3K	MAP kinase kinase kinase
MEK	Mitogen activated protein kinase
MET	Mesenchymal-epithelial transition
mTORC	mechanistic target of rapamycin complex
NOD-SCID	Nonobese diabetic/severe combined immunodeficiency
pRCC	Papillary renal cell carcinoma
RCC	Renal cell carcinoma
OIP5	Opa interacting protein 5
PCR	Polymerase chain reaction
PDGF	Platelet derived growth factor
PDK	phosphoinositide-dependent kinase
PI3K	phosphorylates phosphatidylinositol 3-kinase
PIP_3	phosphatidylinositol (3, 4, 5)-triphosphate
PLK1	Polo-like kinase 1

PTEN	Phosphatase and tensin homolog
Rb	retinoblastoma
TFE3	Transcription factor E3
TGF	Transforming growth factor
TMA	Tissue microarray
TP53	Tumor protein p53
VEGF	Endothelial growth factor
VHL	von Hippel–Lindau
VSC-G	Vesicular stomatitis virus G protein

I. INTRODUCTION

1.1 Renal Cell Carcinoma (RCC)

RCC is originated from renal tubular epithelial cells and accounts for 85% of primary renal neoplasms (Nabi *et al*, 2018)). Based on the study of RCC, the majority of the cancer cases is sporadic and only 2-3% are familial (Nerli *et al*, 2015). Each year, approximately 200,000 new cases and 100,000 deaths are caused by RCC, counting toward 3% of all human cancer (Jonasch *et al*, 2014), and it is among the top 10 common cancers worldwide (Nabi *et al*, 2018). In Canada, RCC was ranked 10th most common cancer in 2019 with estimated 7200 cases a year, and the incidence rate of RCC is approximate twice higher in men than women (Hotte *et al*, 2019). Globally, RCC is the 9th most prevalent cancer in men and ranked 14th in women (Medina-Rico *et al*, 2018). In 2012, RCC leads to estimated 143000 deaths worldwide, making it the 16th most common cause of cancer death (Medina-Rico *et al*, 2018). Smoking, hypertension, obesity, genetics, pollutants, and other pre-existing conditions such as renal transplantation, acquired cystic kidney diseases are considered as the main risk factors for RCC (Chow *et al*, 2010). The recommended methods to prevent RCC are the avoidance of smoking, and well management of hypertension and obesity (Gray and Harris, 2029). CT scans or renal ultrasounds are the common tools for early RCC detection, however, screening of RCC is not recommended unless the patient has known heritable syndrome which associated with RCC (Gray and Harris, 2019).

RCC is asymptomatic in most of early stages, more than half of the RCC patients were diagnosed incidentally from the imaging of other unrelated issues (Campbell *et al*,

2009). Classical symptoms of RCC including gross hematuria, palpable abdominal mass and flank pain, while they are not common and normally associated with advanced RCC stages (Gray and Harris, 2019). The diagnosis of early stage RCC has greatly improved due to the advances of medial imaging techniques of ultrasound, computed tomography (CT) and magnetic resonance imaging (MRI) scan (Gray and Harris, 2019). Ultrasound now is the first imaging option for RCC screening as it lacks radiation and does not need nephrotoxic contrast agents (van Oostenbrugge *et al*, 2018). Besides, ultrasound is relatively low-cost compared to other imaging methods (van Oostenbrugge *et al*, 2018). A CT scan is able to detect 90% of renal mases, as well as identifying pathological features of the mass and evaluate surrounding anatomy (Gray and Harris, 2019). MRI is used to characterize indeterminate RCC tumors on ultrasound (US) and CT, especially when the lesion is concerned to be angiomyolipoma or pRCC. Besides, MRI is also utilized when the patient is contraindicated to CT due to impaired renal function (van Oostenbrugge *et al*, 2018). Even patients with stage I or stage II RCC cancer at the time of diagnosis has a 5-year survival rate over 80%, most of patients are diagnosed at advance stage, and approximate 30% of them develop metastasis with survival rate dropped to 0-20% (Gray and Harris, 2019 & Kalra *et al*, 2016). Treatment for non-metastatic RCC tumor is nephrectomy, preferably in minimal invasive method (Gray and Harris, 2019). The estimated 5-year survival rate for RCC patients treated by partial and radical nephrectomy can reached to 81.5% and 69.5% respectively (Tan *et al*, 2013). For metastatic RCC (mRCC), available interventions include VEGF receptor inhibitors such as sunitinib (Sutent) and pazipanib (Votrient) for first line treatments, Opdivo and Everolimus for second line treatments (Gray and Harris, 2019). However, the treatments for metastatic RCC can only improve overall

survival of the patients for approximate 1.5 years, while the disease cannot be cured (Chen *et al*, 2019).

RCC is a heterogenous disease and it consists of multiple subtypes named by their histopathological characterization (Muglia and Prando, 2015, Table 1). Clear cell RCC (ccRCC), papillary RCC (pRCC), and chromophobe RCC (chRCC) are the three common subtypes of RCC (Sanchez-Gastaldo *et al*, 2017). ccRCC contributes for 75% of all RCC cases and it is originated from epithelial cells of the proximal nephron (Jonasch *et al*, 2014). Clear cytoplasm and nested cluster of cells that are surrounded by mass of endothelial networks are the features of ccRCC (Jonasch *et al*, 2014). 95% of ccRCC cases are developed sporadically, mutation of the *VHL* gene is the major initiation factor of ccRCC. The VHL protein regulates the expression of an oxygen-related cellular response modulator protein: hypoxia-inducible factor (HIF). In normoxic environment, VHL interacts with HIF to promote its ubiquitination, leading to its degradation (Sanchez-Gastaldo *et al*, 2017). However, in a hypoxic situation, deficiency of oxygen leads to the accumulation of HIF, which eventually enhances the transcription of the genes that aid cellular adaption to hypoxia and leads to the up-regulation of endothelial growth factor (VEGF), platelet derived growth factor (PDGF) and transforming growth factor alpha and beta (TGFα & β) (Maxwell *et al*, 1999). Therefore, VHL is a tumour suppressor, and the loss or mutation of *VHL* gene leads to the accumulation of HIF, which promotes angiogenesis, growth and proliferation of tumour cell (Grandinetti and Goldspiel, 2007). Additionally, ccRCC tumor is more aggressive when there are mutations in AKT/PI3K/mTOR signaling pathway (Brugarolas, 2014).

pRCC arises from distal nephron and accounts for 10-15 % of RCC cases. pRCC is a heterogenous disease with 2 major histological subtypes possessed different genetics entities, disease development and patient outcomes (Linehan *et al*, 2015).

Type 1 and type 2 are the two main subtypes of pRCC and they are diagnosed both by their papillary architecture and genetic defects (Jonasch *et al*, 2014). Recent studies on type 1 pRCC genomic characterization have revealed that approximate 81% of the patients containing mutant *MET* gene through various genetic alternation including mutations, gene fusion, splice variants or high copy number of chromosomes 7 (Sanchez-Gastaldo *et al*, 2017). Histologically, type1 pRCC is differentiated by the tubular and papillae structures which is covered by small cells that contain oval nuclei and basophilic cytoplasm (Linehan *et al*, 2015). Type 2 pRCC in part caused by mutations that inactivating the *fumarate hydratase (FH)* gene (Kovacs *et al*, 1991). Prominent nucleoli with large nuclei, as well as papillae structure covered by the cells contains eosinophilic cytoplasm is the unique histological feature of type 2 pRCC (Linehan *et al*, 2015). Patients with pRCCs generally have better prognosis than ccRCCs, and type 1 pRCC carries better prognosis than type 2 pRCC as it is usually detected at lower grades and earlier stages (Muglia and Prando, 2015).

chRCC is relatively rare compared with other two types of RCC, accounting for 5% of all RCC cases (Rathmell *et al*, 2015). chRCC is originated from distal tubule and has distinct morphology from other RCC including empty cytoplasm and reticular pattern (Rathmell *et al*, 2015). Studies have demonstrated a large number of chRCC cases developing *TP53* mutation or losing one copy of the entire chromosome (Rathmell *et al*, 2015). Besides, the PTEN/ mTOR pathway is altered during the development of

chRCC (Rathmell *et al*, 2015).

Less common subtypes of RCC include cystic-solid, collecting duct (Bellini), medullary, xp11 translocation, mucinous tubular and spindle cell, neuroblastoma-associated and non-classified RCC (Muglia and Prando, 2015). The incident of cystic solid ranges from 1% to 4% of all RCCs, appearing as a cystic lesion differentiated from kidney by a fibrous capsule (Muglia and Prando, 2015). Cystic-solid RCC has good prognosis and can be cured without recurrence or metastasis (Muglia and Prando, 2015). Collecting duct RCC counts for less than 1% of RCC cases, while it is highly aggressive with 30% of patients presenting metastasis during diagnosis and more than 60% of them die within two years (Sriglet and Eble, 1998). Medullary RCC is a rare RCC originated in distal nephrons and extremely aggressive (Muglia and Prando, 2015). The association between medullary RCC and sickle cell disease is the unique feature of medullary RCC, and it mainly affects young people between age 30 to 40 (Muglia and Prando, 2015). Xp11 translocation RCC is a rare RCC due to translocation of TFE3 and xp.11.2 chromosome (Decastro and McKiernam, 2008). The disease carries mores indolent prognosis compared to ccRCC and it is more common in young age (Decastro and McKiernam, 2008). Mucinous tubular and spindle cell RCC is a newly described rare disease which originated from distal convoluted tube cells and collecting ducts (Lopez-Beltran *et al*, 2009). Female in their fourth and fifth decade of life are prevalence for mucinous tubular and spindle cell RCC (Lopez-Beltran *et al*, 2009). Neuroblastoma-associated RCC develops in the children who has been treated for neuroblastoma, and such neoplasm develops hypo vascular lesion and more indolent behaviours (Fleitz *et al*, 2003).

The diagnosis of RCC depends on the exclusive clinical criteria and the treatments are limited to nephrectomy (radical or partial), chemotherapy, radiotherapy, and anti-cancer drugs (Marencak, 2017). Due to the heterogeneity of RCC and inadequate biomarkers, it is difficult to accurately categorize the disease and provide tailored therapies to individual patients. Therefore, the needs of RCC biomarkers to precisely identify RCC and optimize treatments are intensified.

Table 1. Classification of RCC

Subtype	Incidence	Origination	Biological behaviour
ccRCC	75%	Proximal nephron	Aggressive based on stage
pRCC	10-15%	Distal nephron	Aggressive based on stage
chRCC	5%	Distal nephron	Less aggressive
Cystic-solid	1%	Proximal nephron	Indolent
Collecting ducts (Bellini)	1%	Collecting tube	Aggressive
Medullary	1%	Distal nephron	Extremely aggressive
Xp11 translocation	Rare	Distal nephron	Indolent
Mucinous tubular and spindle cell	Rare	Distal nephron	Mild
Neuroblastoma-associated	Rare	Proximal nephron	Indolent
Non-classified	4%	Variable	-

1.2 Opa Interacting Protein 5 (OIP5)

OIP5, which is also known as Mis18β and LIN5-25, is a 25-kDa protein that is accumulated in telophase-G1 centromere (Takeshi *et al*, 2004) and plays a critical role in centromere formation (Figure 1). Chromosome segregation requires kinetochore to direct the movements of chromosome by interacting with spindle microtubules (Allshire and Karpen, 2008). The assembly of kinetochores on centromere is specified by nucleosomes with centromere-specific histone H3 variant CENP-A (Allshire and Karpen, 2008). CENP-A is a centromere protein which replaces conventional histone H3 during cell cycle to modify the structure of nucleosome during cell division (Regnier *et al*, 2005). New CENP-A is required in cell cycle since it is the epigenetic marker for centromeric chromatin (Allshire and Karpen, 2008). Mis18α, Mis18β, Mis18 binding protein 1 (Mis18BP1), together with Holliday junction recognition protein (HJURP), are the four core factors of CENP-A localization (Pan *et al*, 2019). Recent studies have demonstrated that Mis18β forms Mis18 heterotetramer with Mis18α and the complex directs the deposition of new CENP-A nucleosome by recruiting HJURP directly to maintain the identity of centromere (Figure 1, Stellfox *et al*, 2016). Besides, Mis18α and Mis18β also interact with Mis18 binding protein 1 (Mis18BP1) and they depend on each other for their localization (Barnhart *et al*, 2011). In addition, centromere protein C (CENP-C) creates an important platform for the kinetochore during mitosis by binding to CENP-A nucleosome (Gascoigne *et al*, 2014). Researches have shown that Mis18β and Mis18BP1 interact with CENP-C directly in a cell cycle dependent manner, together with Mis18α binding to the N-terminus of Mis18BP1, resulting in the full localization of the Mis18 complex and regulation of CENP-A during cell cycle precisely

(Stellfox *et al*, 2016). The deposition of CENP-A is positively and negatively regulated by PLK1 and CDK1/2 respectively (Figure 1, Pan *et al*, 2019). PLK1 interacts with Mis18β in G1 phase for CENP-A localization and Mis18 complex stability (McKinley and Cheeseman, 2015), while CDKs are phosphorylating HUJRP to prevent its binding to Mis18 complex therefore inhibits the localization of CENP-A (Pan *et al*, 2019). In addition, the binding between Mis18 heterotetramer and HJURP leads to dissociation of Mis18α and Mis18β into dimer, therefore their re-binding to centromeres are restricted (Stellfox *et al*, 2016).

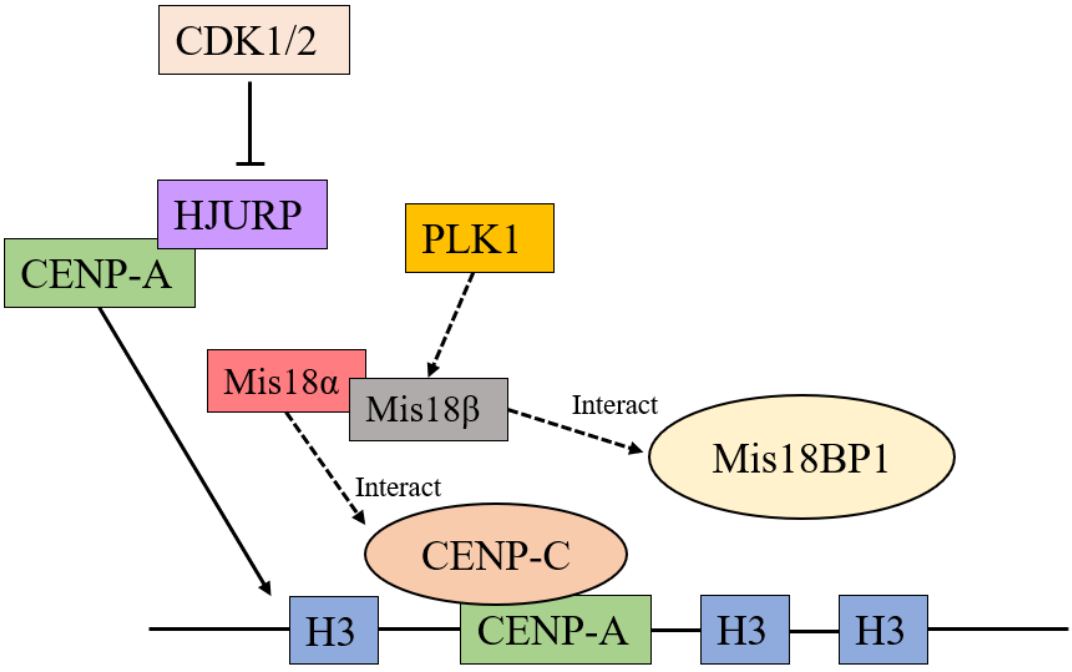

Figure 1. A model indicated the role of OIP5 in cell cycle. OIP5 (Mis18β) forms heterotetramer with Mis18β, and the complex interacts with Mis18BP1 and HUJRP for the localization of CENP-A and CENP-C. PLK1 positively regulates the deposition of CENP-A by interacting with Mis18β, and CDKs negatively regulates the deposition of CENP-A by phosphorylating HUJRP.

CENP-Centromere protein, HJURP- Holliday junction recognition protein, H3- Histone H3, PLK1- Polo like kinase 1, CDK- Cyclin-dependent kinase

1.3 Association between OIP5 and Raf1

OIP5 is reported to interact with various oncogenic proteins including Raf1 and Akt (Yuryex and Wennogle, 2003, Li *et al*, 2017). Raf1, also known as c-RAF, is a MAP kinase kinase kinase (MAP3K) which initiate ERK1/2 activation through activation of MAP kinase kinase MEK1 and MEK2 (Figure 2, Hatzivassiliou *et al*, 2010). c-Raf is also regulated (Hatzivassiliou *et al*, 2010). The inhibition of c-Raf is due the physical interaction between the N-terminal autoinhibitory domain and its kinase domain (Hatzivassiliou *et al*, 2010). Activated G-protein could interfere this intramolecular interaction within Raf1, resulting in a conformation change and activation of Raf1. Active Raf1 eventually becomes dimerized and phosphorylate each other to become fully activated protein kinase (Hatzivassiliou *et al*, 2010). Raf1 dimer then phosphorylates MEK1 and MEK2 protein kinase, leading to the phosphorylation and activation of ERK1/2 and their downstream targets (Figure 2, Hatzivassiliou *et al*, 2010). There are more than 160 downstream molecular targets of ERK1/2, which are involved in multiple cellular processes including cell cycle progression, cell migration, cell differentiation and apoptosis inhibition (Hatzivassiliou *et al*, 2010). Cascade reaction of Ras/Raf/MEK/ERK is associated with cell resistance to chemotherapy (Li *et al*, 2016). Study conducted by McCubrey *et al* discovered that hematopoietic cell with adriamycin and paclitaxel resistance possesses upregulated ERK expression, and the cell is highly sensitive to Raf/MEK inhibitor (McCubrey *et al*, 2007). Besides, re-activation of MEK in MEK gene-deficient cells is able to increase cell's resistance to adriamycin by 10-fold (McCubrey *et al*, 2007). For breast cancer, Raf leads to paclitaxel and doxorubicin resistance through Mdr-1 and Bcl-2 anti-apoptotic proteins (McCubrey

et al, 2007). Therefore, Raf1 plays critical roles in triggering cell signaling responses, and its expression is correlated with tumor growth, metastasis and drug resistance (Hatzivassiliou *et al*, 2010). Raf1 is highly expressed in wide range of tumors, and it triggers a cascade of cell signaling responses which enhance the survival of tumor cells (Koinuma *et al*, 2012). Studies conducted by Koinuma *et al* demonstrated that Raf1 directly interacts with OIP5 and regulates the stability of OIP5 in lung cancer (Figure 2, Koinuma *et al*, 2012). The level of OIP5 can be controlled by changing Raf1 expression, OIP5 expression level is decreased when Raf1 is silenced while the level of *OIP5 mRNA* unchanged (Koinuma *et al*, 2012).

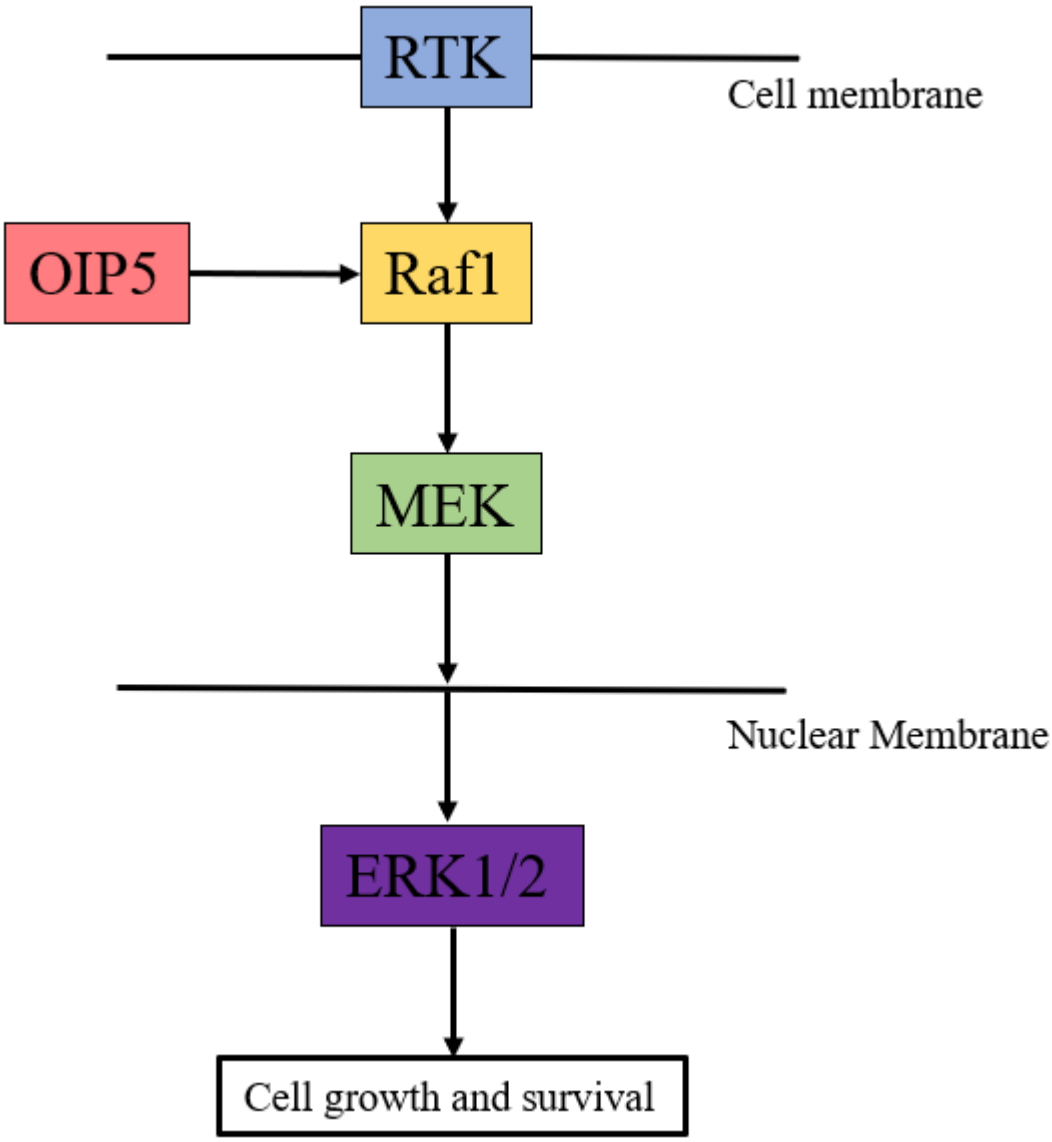

Figure 2. A model indicated the role of OIP5 involved in MAPK pathway. Binding of OIP5 enhances Raf1 activity in the phosphorylation and activation of ERK1/2 pathway, leading to tumor cell growth and survival.

RTK-receptor tyrosine kinase, OIP5-opa interacting protein 5, MEK- mitogen extracellular kinase, ERK- extracellular signal-related kinase.

1.3 Association between OIP5 and Akt

In addition to Raf1, OIP5 is associated with cancer development by activating Akt through the mTORC2 and p38/PTEN pathways (Figure 3, Li *et al*, 2017). Akt signaling pathway plays an important role in cell growth and proliferation by responding to extracellular signals (Manning and Cantley, 2007). Growth factor activates the receptor tyrosine kinase on cell surface, therefore phosphorylates phosphatidylinositol 3-kinase (PI3K) (Manning and Cantley, 2007). Activated PI3K forms second messenger phosphatidylinositol (3, 4, 5)-triphosphate (PIP_3) by phosphorylating lipids on the plasma membrane (Manning and Cantley, 2007). Serine/Threonine kinase Akt is then translocated to the plasma membrane by interacting with PIP_3 and get partially activated by phosphoinositide-dependent kinase 1 (PDK1) on phosphorylation site Thr308 (Manning and Cantley, 2007). Complete activation of Akt required phosphorylation on S473, which involves phosphoinositide-dependent kinase 2 (PDK2), integrin-linked kinase (ILK), mechanistic target of rapamycin complex (mTORC) and DNA-dependent protein kinase (DNA- PK). The activation of Akt occurs downstream of mTORC2 and upstream of mTORC1 (Li *et al*, 2017). Akt controls downstream cell responses including cell growth, survival, migration, and angiogenesis through phosphorylation of its target (Manning and Cantley, 2007). These actions contribute to Akt's oncogenic functions (Manning and Cantley, 2007). Research indicated overexpression of OIP5 increases the phosphorylation of Akt while knockout of OIP5 leads to a decrease of Akt level in liver cancer (Li *et al*, 2017) Elevated expression of OIP5 increases the phosphorylation of Akt by upregulating mTORC2 signalling pathways, as well as downregulating p38 and PTEN activity (Figure 3,Li *et*

al, 2017). Akt is linked to mTORC signaling, and it is negatively regulated through converting PIP_3 into PIP_2 by PTEN, a tumor suppressor (Brito *et al*, 2015). The downregulation of PTEN results in Akt activation, leading to the activation of mTORC signalling pathway which is highly related to cancer development (Hua *et al*, 2017). Akt controls β-catenin-dependent transcription by directly activating β-catenin or inhibiting GSK-3β. Upregulation of OIP5 increases the phosphorylation of GSK-3β and β-catenin, leading to enhanced phosphorylation of two well established cell cycle regulators, Cdc2 and Cdc25C (Li *et al*, 2017). In addition, the activation of mTORC1 by OIP5 is associated with tumor proliferation during G_1/S cell cycle progression and metastasis (Li *et al*, 2017). Besides, the activation of Akt triggers the translocation of β-catenin, which acts as a transcription factors of Myc and cyclin D1, to enhance the development of cancer (Li *et al*, 2017).

OIP5 is extensively expressed in testis, and recent studies have proposed that *OIP5* gene is a cancer-testis specific gene (Zhang *et al*, 2017). OIP5 has been found to be upregulated and contributes to the malignancy of kidney, gastric, colorectal, lung and esophageal cancers (Li *et al*, 2018). Besides, various studies have indicated that OIP5 could interact with Raf1 and Akt to promote the development of cancer by taking the advantage of the activation of Raf1 and Akt downstream genes, promoting the proliferation, survival and angiogenesis of cancer cell (Li *et al*, 2018). Knockout of OIP5 inhibits cell growth cell apoptosis in colorectal and gastric cancer (Chun *et al*, 2010). Therefore, OIP5 may play a role in RCCs.

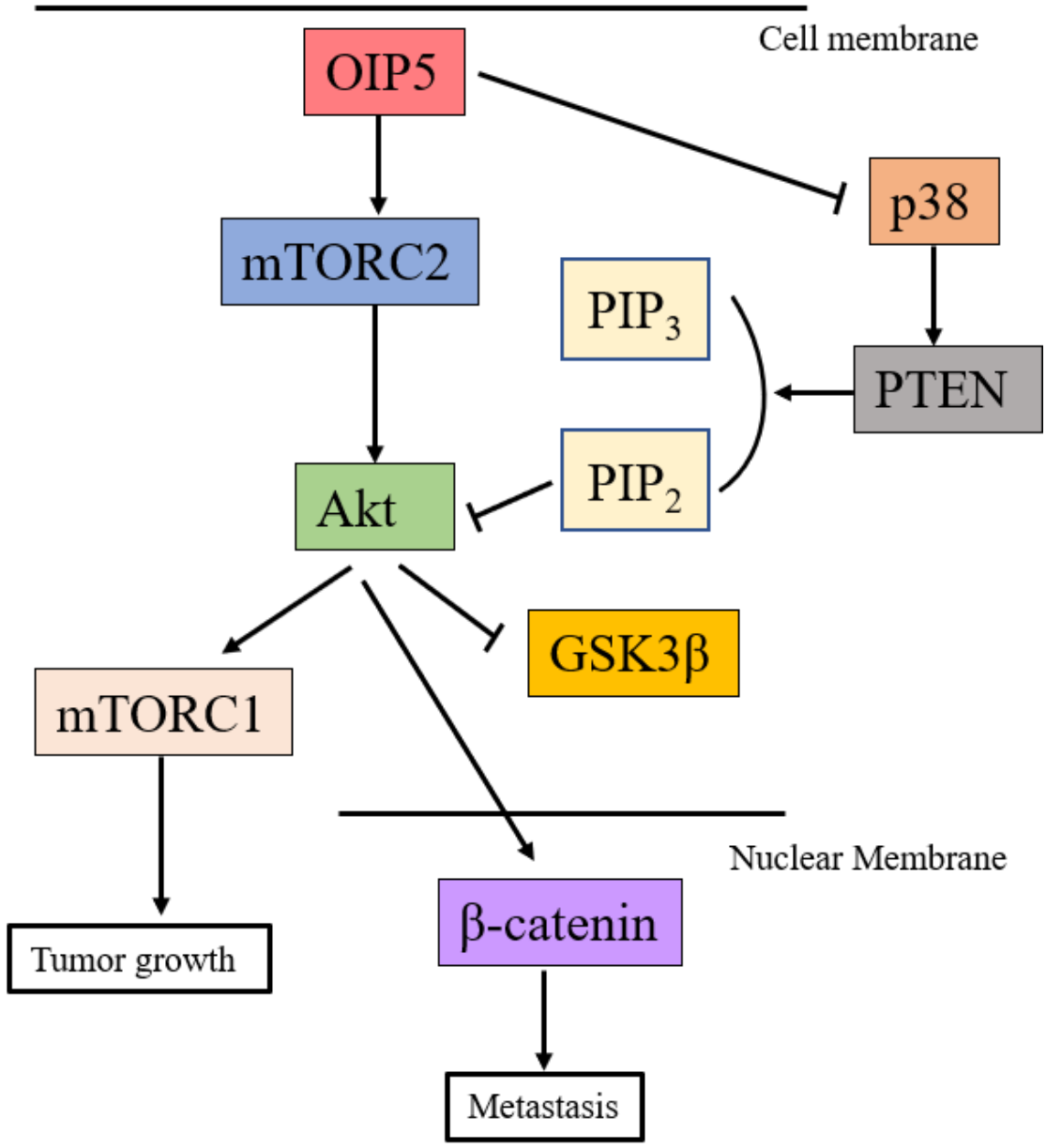

Figure 3. A model indicates the role of OIP5 in activating Akt through mTORC2 and p38/PTEN pathway. Elevated expression of OIP5 increases the phosphorylation of Akt by upregulating mTORC2 signalling pathways, as well as downregulating p38 and PTEN activity. Upregulation of Akt increases the phosphorylation of GSK-3β and β-catenin, leading to enhanced tumor growth and metastasis.

mTORC- mammalian target of rapamycin complex, PTEN- Phosphatase and tensin homolog, Akt- Protein kinase B, GSK-3β- Glycogen synthase kinase 3 beta, PIP_3- Phosphatidylinositol (3,4,5)-trisphosphate, PIP_2- Phosphatidylinositol 4,5-bisphosphate

Adapted from Li *et al*, 2017

1.4 Polo-like kinase 1(PLK1)

PLK1, or as serine/threonine-protein kinase 13 (STPK13), which belongs to the family of serine/threonine protein kinases (Liu *et al*, 2017). Among the five members of human *PLK* family, which are *PLK1, PLK2, PLK3, PLK4* and *PLK5, PLK1* is the most intensively studied member (Liu *et al*, 2017). PLK1 protein possesses a N-terminal kinase catalytic domain and a C-terminal polo-box domain (Liu *et al*, 2017). The T-loop of the N-terminal catalytic domain of PLK1 is linked to its kinase activity, and C-terminal polo-box domain allows PLK1 to bind to phosphopeptide of certain proteins (Liu *et al*, 2017).

PLK1 is required throughout mitosis and plays pleiotropic roles including kinetochore function, mitotic spindle formation, centrosome maturation, and cytokinesis (Schmucker and Sumara, 2014). PLK1 controls bipolar spindle assembly during prometaphase and supports kinetochore-microtubule attachment. During cell cycle progression, M-phase promoting factor (MPF), which is a complex of a cyclin-dependent kinase CDC2/cyclinB, is required to initiate mitosis (Toyoshima-Morimoto *et al*, 2002). PLK1 triggers G2/ M phase transition by phosphorylating and activating CDC25C, resulting in the phosphorylation and activation of CDC2/CyclinB (Sur and Agrawal, 2016). The kinase activity retains until telophase where PLK1 participates in the completion of cytokinesis, and PLK1 is later degraded by anaphase promoting complex/cyclosome (APC/C) E3-ubiquitin ligase1 (Sur and Agrawal, 2016).

Studies have demonstrated that PLK1 is a proto-oncogenic protein. PLK1 is upregulated in multiple cancer including lung, bladder, and kidney cancer (Carcer, 2019). The expression of PLK1 is associated with p53, a potent tumor suppressor

(Carcer, 2019). Mutation in *p53* gene or silenced p53 commonly occurs in malignancies (Carcer, 2019). The expression of PLK1 is modulated by cell cycle-dependent element/cell cycle genes homology region (CDE/CHR) cell cycle regulation binding sites harboured on PLK1 via p53 effector, p21 (Carcer, 2019). The expression of PLK1 is reduced by binding to p21 (Carcer, 2019). Therefore, impaired p53 results in elevated PLK1 expression, leading to genomic instability and oncogenesis (Carcer, 2019). In addition to p53, PLK1 can also modulate the expression of a tumor suppressor, phosphatase and tensin homolog (PTEN) (Carcer, 2019). PTEN possess functions in the nucleus (Carcer, 2019). PLK1 phosphorylates PTEN, leading to the inhibition of PTEN mono-ubiquitination and thereby preventing PTEN to enter nucleus (Carver, 2019). Research on the clinical implication of PLK1 inhibitor is emerging, and there are several PLK1 inhibitors are currently under clinical trail including BI 2536, GSK461364A, Rigosertib and volasertib, with BI 2536 been the first and most widely studied one (Yim, 2013).

1.5 Association between OIP5 and PLK1

In eukaryotes, centromere is epigenetically featured by histone H3 variants CENP-A, which replaces histone H3 in centromeric chromatin and participates in cell cycle progression activities including kinetochore assembly and chromosome stability (Valdivia *et al*, 2009). The deposition of CENP-A requires precise regulation since dysfunctional centromere may result in chromosome loss, chromosome mis-segregation and DNA damage (McKinley and Cheeseman, 2015). Research has demonstrated that PLK1 acts as a centromere localization regulator for CENP-A deposition in a Mis18

complex-dependent manner, and PLK1 is necessary to maintain Mis18 complex localization during G1 phase (McKinley and Cheeseman, 2015). Besides, Mis18β (OIP5) also maintain its protein stability by interacting with PLK1 (Liu *et al*, 2013). Therefore, PLK1 has the potential to be a promising therapeutic target for the tumor with OIP5 overexpression.

II. HYPOTHESIS AND OBJECTIVES

Studies have proven the association between OIP5 and multiple cancers including kidney, gastric, colorectal, lung and esophageal, and bladder (Gong *et al*, 2013; Chun *et al*, 2010; Li *et al*, 2019; Wang *et al*, 2018). Upregulation of OIP5 is related to tumor growth, poor prognosis metastasis and drug resistance in cancer (; Wang *et al*, 2018). However, the involvement of OIP5 in RCC has only been limited studied. PubMed listed one article under "OIP5 AND renal cell carcinoma" on Oct 15, 2020. The contributions of OIP5 to pRCC has not be reported.

We thus hypothesize contributions of OIP5 to RCC pathogenesis

The objectives of this study are to investigate the role of OIP5 during the development of RCC with a focus on ccRCC and pRCC. Specifically, this study will

1. Examine the oncogenic activities of OIP5 towards ccRCC (A498 and 786-O) and pRCC (ACHN) cells *in vitro* and *in vivo*
2. Determine the clinical relevance of OIP5 with respect to its expression and its association with prognosis
3. Investigate whether OIP5 or its related signaling can be explored to inhibit RCC

III. MATERIALS AND METHODS

3.1 Materials

Ampicillin, aprotinin, calcium chloride ($CaCl_2$), crystal violet dimethyl sulfoxide (DMSO), phenylmethysulfonyl fluoride (PMSF), sodium dihydrogen orthophosphate (NaH_2PO_4), disodium dihydrogen orthophosphate ($Na_2H_2PO_4$), dipotassium hydrogen orthophosphate (K_2HPO_4), EDTA, Tween 20, potassium acetate, potassium chloride, ammonium per sulphate (APS), β-mecaptoethanol, Tween-20, potassium chloride, sodium bicarbonate ($NaHCO_3$), ethanol, aprotinin, leupeptins were purchased from Sigma, Oakville, ON. TEMED, Tris, agarose, sodium bovine serum albumin (BSA), glycine, sodium dodecyl sulphate (SDS), sodium chloride (NaCl), sodium citrate, hydrogen chloride (HCl) were purchased from Bioshop Burlington, ON. 30% acrylamide solution was purchased from Bio-rad, Mississauga, ON. Typsine-EDTA, Superscript were purchased from Invitrogen, Carlsbad, CA. Methanol, xylene, and isopropyl alcohol were purchased from Caledon Laboratories, Georgetown, ON. Ethanol, TRIzol, SYBR Green was purchased from Fisher Scientific, Ottawa, ON. DAB and ABC were purchased from Vector Laboratories, Burlingame, CA. Mini plasmid kit was purchased from Geneaid, New Taipei City, Taiwan. Gel extraction kit was purchased from QIAGEN, Toronto, ON.

3.2 Methods

3.2.1 Tissue culture

A498, ACHN and 786-O cells were obtained from ATCC. A498, ACHN cells were cultured in MEM and 786-O cells was cultured in RPMI1640, both supplemented with 1% Penicillin-Streptomycin (Invitrogen, Carlsbad, CA) and 10% fetal bovine serum (Life Technologies, Burlington, ON). The cell culture was maintained at 37℃ in 5% CO_2 and 95% air with humidity. In the study, A498 and 786-O cell are employed as the model for ccRCC and ACHN is employed as pRCC model.

3.2.2 Plasmids

A plasmid with OIP5 human tagged open reading frame (ORF) clone was obtained from Origene (Cat: RG202255, Rockville, MD). Vesicular stomatitis virus G (VSV-G) and gag-pol (GP) plasmids were purchased from Agilent Technoligies (Mississauga, ON). pBABE-puro plasmid was a gift from Dr. Tak Mak at University of Toronto.

3.2.3 Construction of OIP5 overexpression stable cell lines

The OIP5 ORF was released from its original plasmid by BamHI and PmeI, and pBABE-Flag was linearized by BamHI and EcoRI, followed by converting EcoRI-cleaved end to blunt end. OIP5 was then inserted into pBABE-Flag by rapid DNA

ligation kit (Roche, Mississauga, ON). The 293T cells were transfected by pBABE-OIP5-Flag combined with retrovirus helper plasmid of GP and VSV-G. The medium was changed 12hrs after transfection and the supernatant with retrovirus was harvested after 48hrs. The supernatant was filtered by 0.45μm filter (PALL, Mississauga) and centrifuged in 20000rpm for 1.5hrs at 4℃ to concentrate the retrovirus. Retrovirus was then re-suspended in the corresponding medium. A498, ACHN and 786-O were infected by the viral medium for 1hr. Cells were selected 24 hrs after the infection by 3μg/mL puromycin, and the survived clones were expanded. Positive phenotypes of the stable lines were confirmed by wester blot analysis for Flag and OIP5 protein expression. A498 EV, A498 OIP5, ACHN EV, ACHN OIP5, 786-O EV, 786-O OIP5 were constructed in the study.

3.2.4 Protein extraction and Western blot analysis

Cells were lysed by cell lysis buffer containing 50mM Tris-HCl (pH 7.4- 7.5), 5mM EDTA, 150Mm NaCl, 1% Triton X-100, 1mM NaF, 10% Glycerol, 1mM β-glycerophophate, 1mM PMSF, 100μM Sodium orthovanadate (Na_3VO_4), 2 μg/mL leupeptin and 10 μg/mLaprotinin for 30mins and centrifuged at 14,000 rpm for 10mins at 4℃. An equal amount of protein was obtained from the supernatant of the sample and dilute in water with 5XPSB. The samples were boiled in 100℃ for 5mins before loading. Equal amounts of samples were loaded onto 12.5% SDS-PAGE gels for electrophoresis and transferred onto nitrocellulose membranes (Amersham). The membranes were block by 5% skim milk (Carnation) at room temperature for 1hr, followed by incubating Primary OIP5 antibody (1:500, Sigma-Aldrich) overnight at 4℃

with agitation. Anti-rabbit secondary antibodies with a concentration of 1:2000 diluted in 5% milk were applied to the membrane for 1hr at room temperature. The membranes were then developed by enhance chemiluminescence (ECL) (Amersham) and visualized on X-ray film. The expression of protein was assessed to confirm the expression of OIP5 and Flag.

3.2.5 Colony formation assay and cell proliferation assay

Colony formation assay was conducted by seeding cells in six-well plates with 100, 500, 1000 cells for A498 and ACHN, 100, 300, 500 for 786-O respectively. Colonies were fixed by fixation buffer (2% formaldehyde) and stained by crystal violet (0.5%) after cultured for 2 weeks. Colony numbers and sizes were counted and analysed.

Cell proliferation assay was performed by seeding cells into six-well plate (10^5 per well) and counted the number of cells every two days.

3.2.6 Soft agar assay

1.2% soft agar was dissolved in complete tissue culture medium and 2mL was firstly coated at bottom of six-well plates. Cells in the concentration of 10^5 cell/well and 10^6 cell/well in 2mL of 0.7% agar were dissolved in complete medium were then seeded on the top of the solidified bottom layer. Cells were cultured for approximate 5 weeks with 100μL complete medium added weekly in the same incubation condition as tissue culture.

3.2.7 Invasion Assay

Transwell with insert chamber was used for invasion assay. Insert chamber with control membrane or Matrigel membrane (8-µM pore size) for 24-well plates were purchased (Life Sciences Corning® BioCoat™, USA). Invasion assay was conducted according to the manufacturer's instructions. Cells were starved for 12 or 24hrs and 10^4 cells were seeded into the insert chamber with serum-free medium. Complete medium (10% FBS, 1% Penicillin-Streptomycin) was added to the bottom of 24-well plates. Cells passed through the membrane were fixed by fixation buffer (2% formaldehyde) and stained by crystal violet (0.5%) after 24 or 48 hrs of incubation under the same condition as tissue culture.

3.2.8 Cell cycle distribution

ACHN EV and ACHN OIP5 cell cycle were determined by staining cell with propidium iodine (PI) solution (Sigma) for 1hr (1µg/mL PI and 10 µg/mL RNase in PBS), followed by the examination of cell cycle profile by FACSCelesta. The data was collected by BD FACSDiva Software and analyzed by FlowJo10. ACHN EV and ACHN OIP5 cells were treated in 40nM PLK1 inhibitor (BI2536, Selleckchem) for 72 hrs, and the cell cycle distribution was determined by staining cell with propidium iodine (PI) solution (Sigma) for 1hr, followed by the examination of cell cycle profile by FACSCelesta. The data was collected by BD FACSDiva Software and analyzed by FlowJo10.

3.2.9 Generation of ACHN cell-derived xenograft tumor

ACHN OIP5 and ACHN EV were suspended in 0.1ml MEM/Matrigel (BD) mixture with 1:1 volume and implanted subcutaneously into the left flank 8-week-old non-obese diabetic/severe combined immunodeficiency (NOD/SCID) male mice (The Jackson Laboratory). The mice were carefully monitored one week after the injection through observation and palpation, and the size of the tumor was measure weekly by calipers. Tumor volume was calculated based on the formula $V= L \times W^2 \times 0.52$. The mice were euthanized when the tumor volume reached $1000mm^3$. The xenograft tumor, together with all the major organs, were photographed and collected. All tumors were cut in half, one half was fixed with 10% formalin (VWR, Wester Chester, PA), and the other half was stored in -80 ℃. The formalin fixed tissue was processed by department of Histology, St. Joseph's Health care, Hamilton, ON. The processed tissues were then embedded in paraffin. All the animal works were performed according to the protocols approved by McMaster University Animal Research Ethics Board.

3.2.10 Immunohistochemistry

Kidney cancer TMA (KD29602) was purchased from US Biomax (Rockville, MD). Slide was baked at 60°C for 1 hr, then de-paraffinized in 100% xylene and 70% EtOH series. Antigen retrieval buffer was prepared with sodium citrate buffer (PH=6) in the steamer for 20 minutes. Slide was blocked in the solution with 1% BSA and 10% normal goat serum. OIP5 (Sigma-Aldrich) antibodies with a concentration of 1:50 were incubated at 4℃ over night. Secondary anti-rabbit antibodies with a concentration of

1:200, ABC and DAB solution (5mins) were added to the slides and incubated followed by the IHC protocol. Washes were performed by 1X PBS and distilled water. Slide had been counterstained by haematoxylin for 20 seconds and image analysis was conducted by ImageScope software (Leica Microsystems Inc). Staining intensity scores were calculated into HScore by the formula [HScore= (%Positive) x(Intensity)+1]. Statistical analysis was performed by student t-test, and $p<0.05$ was considered statistically significant.

Xenograft tumors were paraffin embedded and cut serially by microtome. Slides were de-paraffinized in 100% xylene and 70% EtOH series. Antigen retrieval buffer was prepared with sodium citrate buffer (PH=6) in the steamer for 20 minutes. Slide was blocked in the solution with 1% BSA and 10% normal goat serum. OIP5 (Sigma-Aldrich), Anti-Phospho-Histone H3 (Ser 10) (Upstate Biotechnology Inc), CDK2 (Santa Cruz), and PLK1 (Novus Biologicals) antibodies with a concentration of 1:50, 1:200, 1:200, 1:300 respectively, were incubated at 4℃ over night. Secondary antibodies with a concentration of 1:200, ABC and DAB solution (5mins) were added to the slides and incubated followed by the IHC protocol. Washes were performed by 1X PBS and distilled water. Slide had been counterstained by haematoxylin for 20 seconds and image analysis was conducted by ImageScope software (Leica Microsystems Inc). Staining intensity scores were calculated into HScore by the formula [HScore= (%Positive) x(Intensity)+1]. Statistical analysis was performed by student t-test, and $p<0.05$ was considered statistically significant.

3.2.11 Real-time PCR (RT-PCR)

Total RNA was isolated by TRIZOL, and reverse transcription was conducted through Superscript III (Thermo Fisher Scientific) according to the manufacturer's instructions. Quantitative real-time PCR was performed by ABI7500 Fast Real- Time PCR System (Applied Biosystems) using SYBR-green (Thermo Fisher Scientific). All experiments were repeated three times. RNA expression of CENP-A, AURKB, PLK1, CCNB2, CDK1, BUB1 were examined for ACHN EV and ACHN OIP5 xenograft.

Primers used for RT-PCR

CENP-A-FW: ACA AGG TTG GCT AAA GGA

CENP-A-RV: ATG CTT CTG CTG CCT CTT

AURKB-FW: TCT CTA AGG ATG GCC CAG AA

AURKB-RV: GCT CAT GAG GAC AAG TGC AG

PLK1-FW: CCT CCG GAT CAA GAA GAA TG

PLK1-RV: AGC AGC TCG TTA ATG GTT GG

CCNB2/CyclinB2-FW: TTC AAC CCA CCA AAA CAA CA

CCNB2/CyclinB2-RV: CTC AGG TGT GGG AGA AGG AC

CDK1-FW: TGG ATC TGA AGA AAT ACT TGG ATT CTA

CDK1-RV: CAA TCC CCT GTA GGA TTT GG

BUB1-FW: AAC AAC CTG CTC AAC ATC AAC

BUB1-RV: GAG TGA TAT CTT CAG CTT GTG

3.2.12 Statistical analysis

Two-tailed Student t-test, one-way ANOVA and two-way ANOVA were performed for statistical analysis of two and more than two groups respectively, with $p<0.05$ to be considered statistically significant. Tukey's test was performed for post-hoc analysis. Statistical analysis is conducted by GraphPad Prism 7 and data are demonstrated as mean ± SD.

IV. RESULTS

4.1 Promotion of pRCC cell proliferation by OIP5

To investigate the effects of OIP5 in RCC cell proliferation, I have established empty vector (EV) and Flagg-tagged OIP5 stable lines in A498, 786-O, and ACHN (Figure 3). The stable expression of ectopic OIP5 was confirmed by Western blot using anti-FLAG and anti-OIP5 antibodies (Figure 4). Based on the anti-OIP5 Western blot (Figure 4, middle panel), ectopic OIP5 was expressed to 2.86, 1.45, and 1.42-fold in ACHN, A498, and 786-O cells respectively in comparison to their respective EV lines.

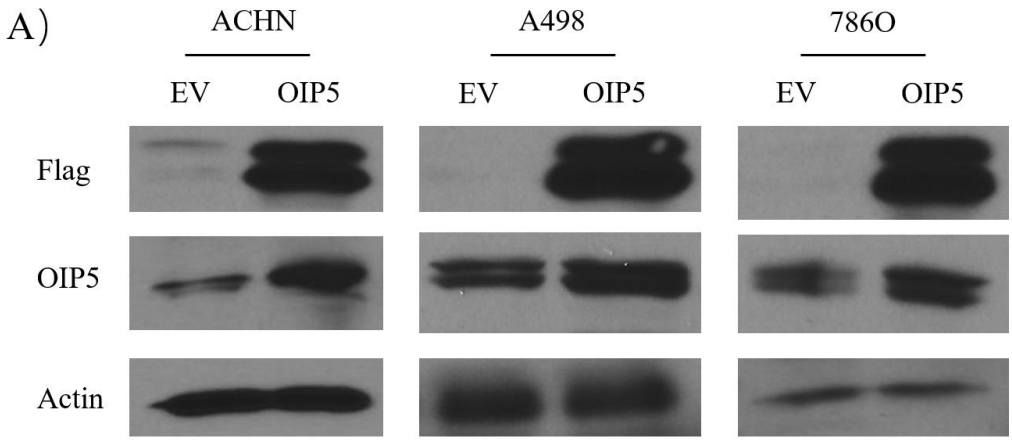

Figure 4. Stable expression of OIP5 in ACHN, A498 and 7860 OIP5 stable cell lines. ACHN, A498 and 7860 cells were stably transfected with an empty vector (EV) or OIP5 retrovirus. The expression of FLAGG-tagged ectopic OIP5 was detected by Western blot analysis using anti-FLAGG and anti-OIP5 antibodies. Actin was used as the loading control. The levels of OIP5 expression in the respective OIP5 stable lines were determined by normalizing the OIP5 band to the respective actin band (middle panel).

Cell proliferation assays on A498, 786O and ACHN stable lines were conducted. Ectopic expression of OIP5 does not affect the proliferation of A498 and 786-O cells compared to the respective EV lines (Figure 5A and 5B). However, enforced OIP5 expression significantly enhance ACHN cell proliferation in comparison to ACHN EV cells (Figure 5C). The underlying reasons for OIP5 differentially affecting pRCC and ccRCC cell proliferation are not clear. It is apparent that ectopic OIP5 could not be expressed in ccRCC A498 and 786-0 cells to a higher level as it in ACHN cells (Figure 4), which might be a contributing factor (see Discussion for details).

A)

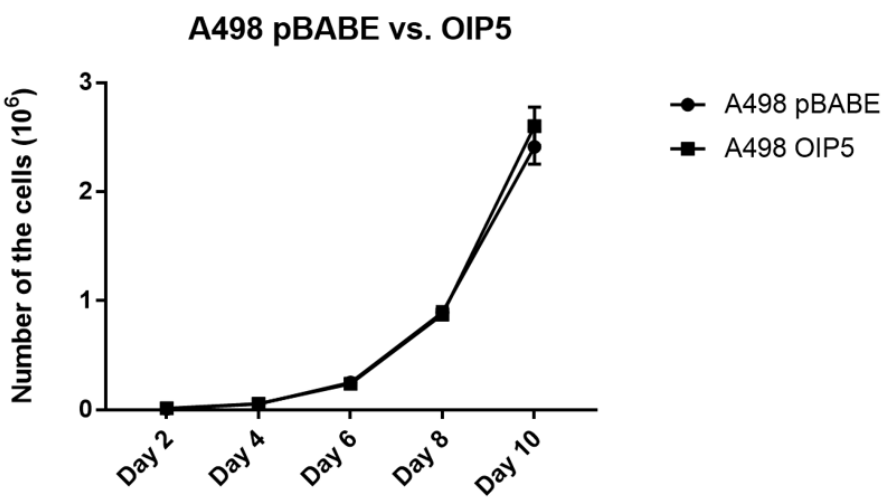

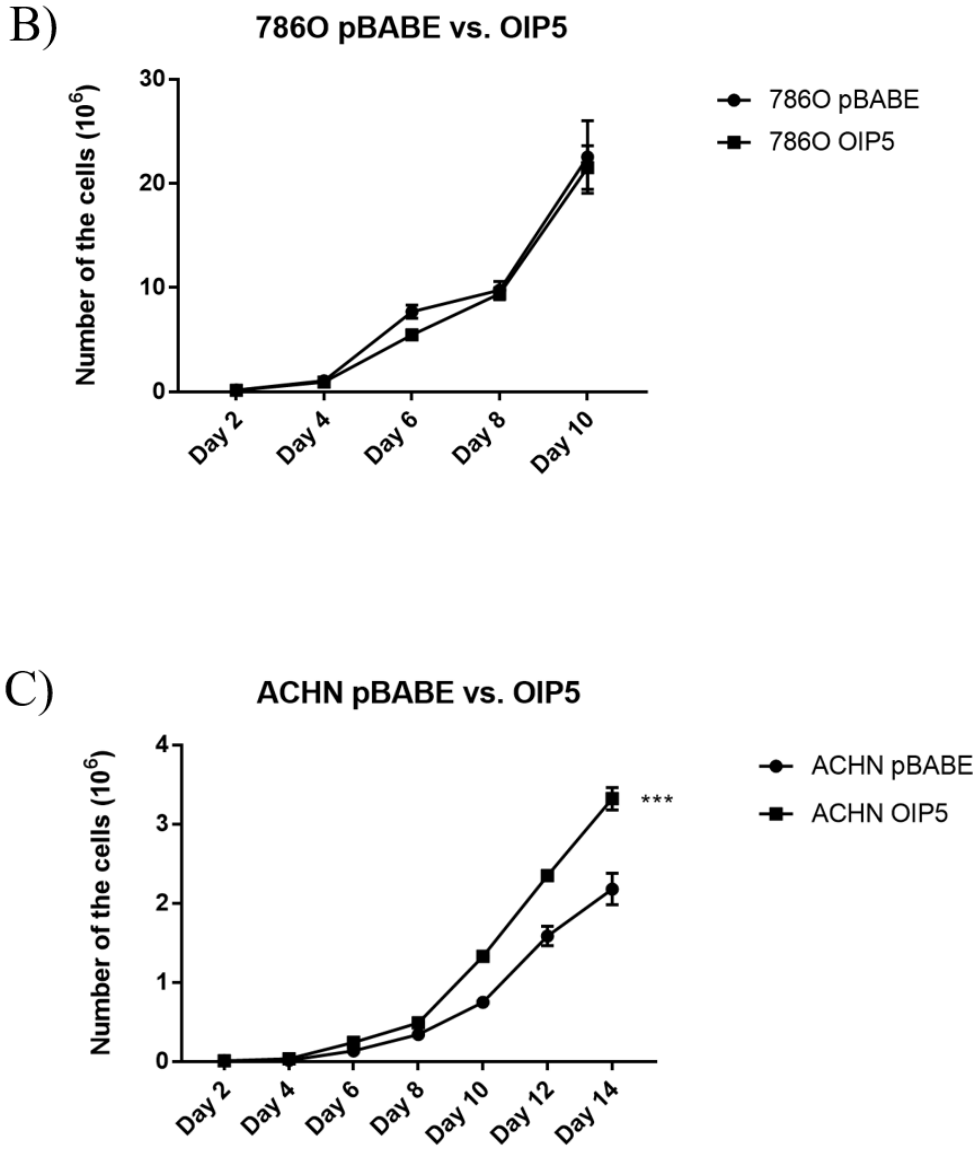

Figure 5. Cell proliferation assay of RCC stable cell lines with OIP5 overexpression. A) Cell proliferation assay of A498 EV and A498 OIP5. B) Cell proliferation assay of 786O EV and 786O OIP5. C) Cell proliferation assay of ACHN EV and ACHN OIP5. Experiments were repeated three times. In day 10, 12, 14, cell numbers of ACHN OIP5 is significantly higher than ACHN pBABE. Two-way ANOVA was conducted for the analysis. All data are presented as mean ± SE. * indicates significant different between ACHN OIP5 and ACHN EV, * when $p \leq 0.05$, ** when $p \leq 0.01$, *** when $p \leq 0.001$, **** when $p \leq 0.0001$.

To further analyze the proliferative effects of OIP5, colony formation assay was performed on A498, 786-O and ACHN stable lines (Figures 6, 7, 8). In different seeding densities used, ACHN OIP5 cells formed significantly more colonies compared to ACHN EV cells (Figure 6). The average numbers of ACHN OIP5 colonies were 72± 4, and 114± 2 for 500 and 1000 cell seeded respectively, which were approximately 2-fold more than ACHN EV with 26± 1 and 52± 5 colonies when 500 and 1000 cells were seeded respectively. However, there were no significant difference between A498 and 786-O stable lines for their colony formation ability (Figure 7 & 8). The colony number of 500 786O cells seeded was not available since the colonies were too many to be counted. These observations are in line with outcomes obtained using proliferation assay (Figure 5). Collectively, we demonstrated that overexpression of OIP5 enhances pRCC ACHN cell but not ccRCC (A498 and 786-0) cell proliferation through multiple in vitro approaches.

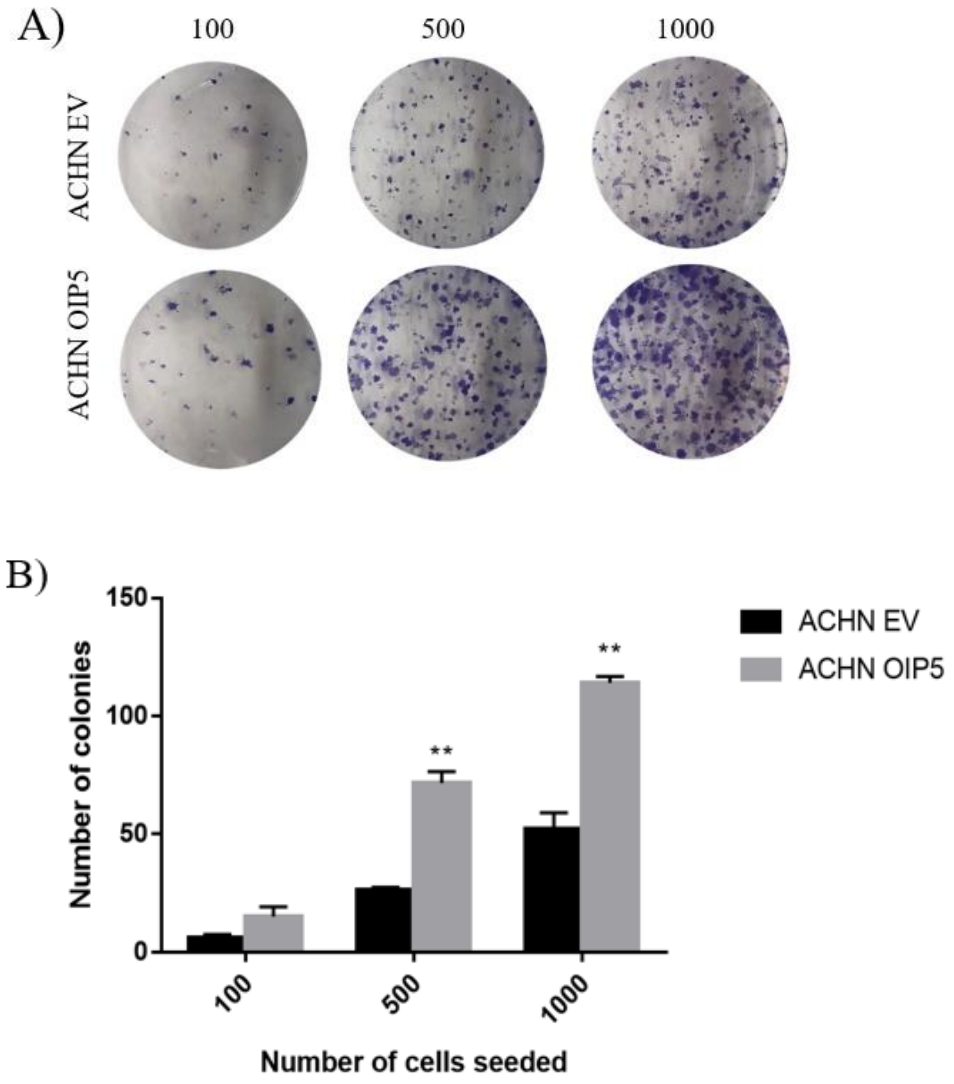

Figure 6. Colony formation assay on solid surface for ACHN stable lines. A) Colony formation assay of ACHN stable lines. B) Colony formation analysis of ACHN stable lines. Experiments were repeated three times. Student t-test was conducted for the analysis. All data are presented as mean ± SE. * indicates significant different between ACHN OIP5 and ACHN EV, * when $p \leq 0.05$, ** when $p \leq 0.01$, *** when $p \leq 0.001$, **** when $p \leq 0.0001$.

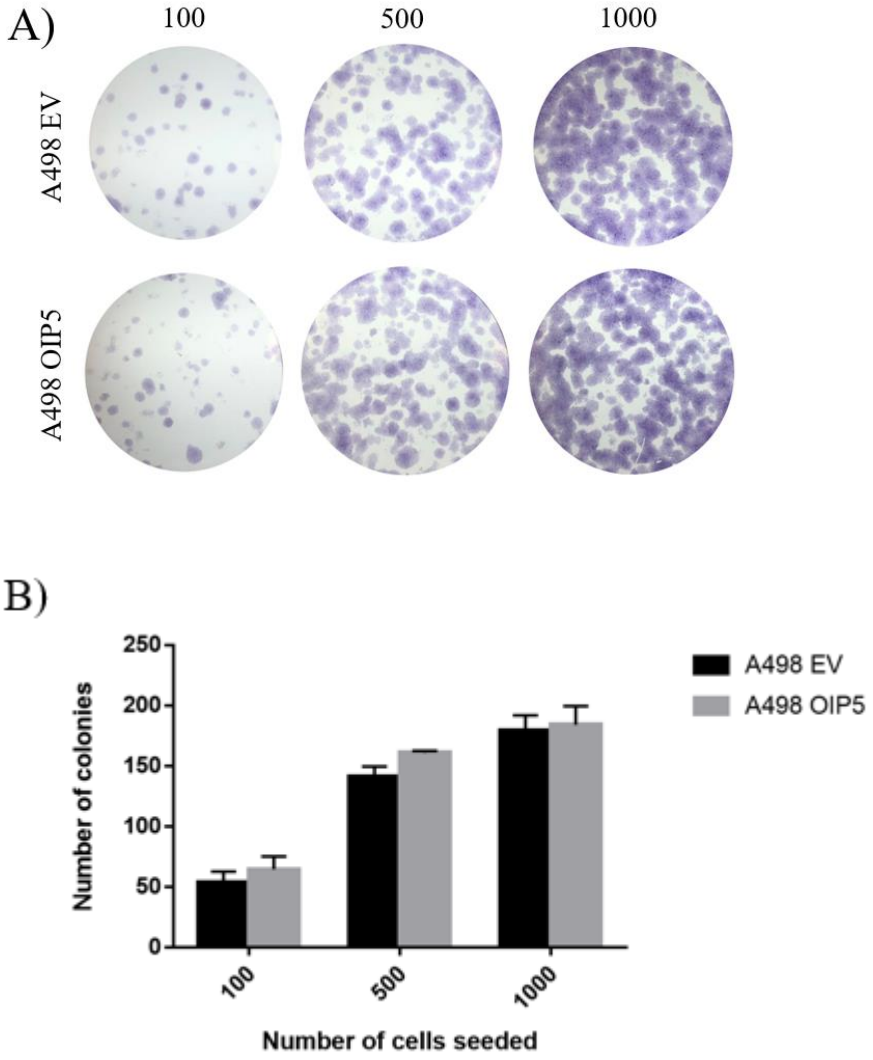

Figure 7. Colony formation assay on solid surface for A498 stable line. A) Colony formation assay of A498 stable lines. B) Colony formation analysis of A498 stable lines. Experiments were repeated three times. Student t-test was conducted for the analysis. All data are presented as mean ± SE.

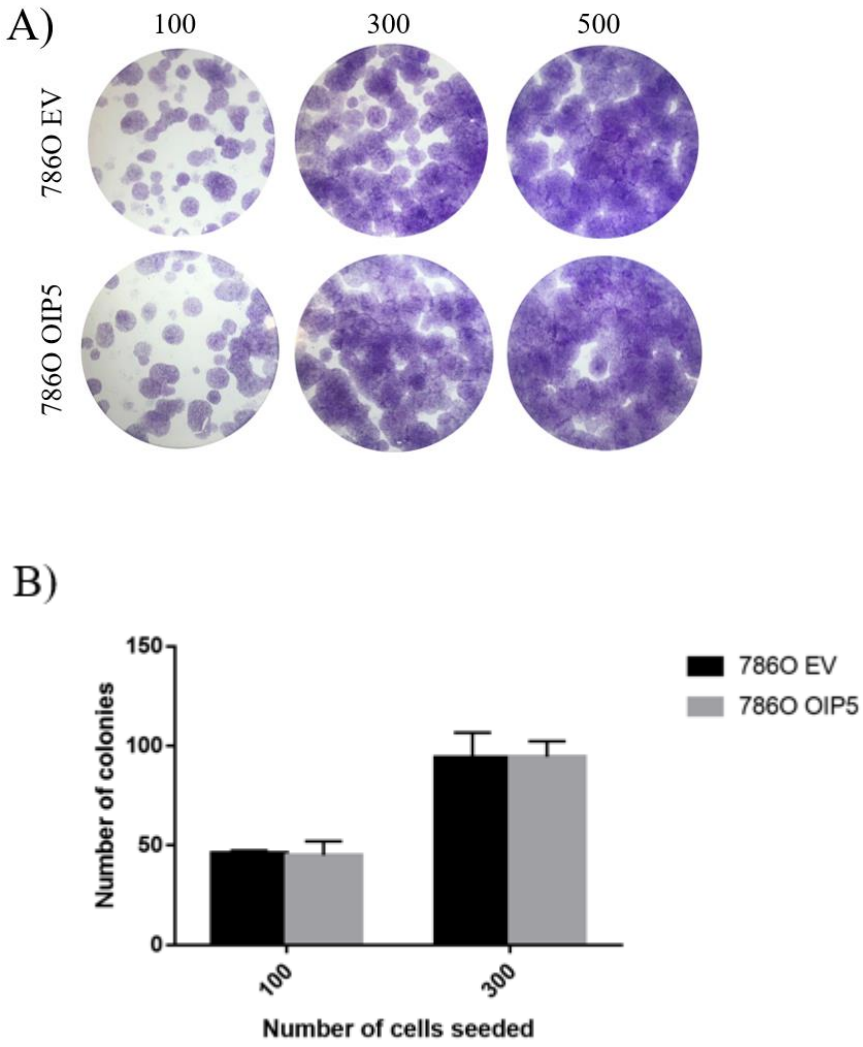

Figure 8. Colony formation assay on solid surface for 786O stable lines. A) Colony formation assay of 786O stable lines. B) Colony formation analysis of 786O stable lines. The data for the colony number of 500 cells seeded is not available because the colonies are too many to be counted. Experiments were repeated three times. Student t-test was conducted for the analysis. All data are presented as mean ± SE.

Given the promotion of pRCC ACHN cell proliferation as monolayer by OIP5, we then analyzed the situation of ACHN cell proliferation under an anchorage-independent environment. Soft agar colony formation assay was utilized in this project to study the anchorage-independent growth of ACHN EV and ACHN OIP5 (Figure 9). After incubation for approximately one month, the average number of colonies in soft agar is 0.67 ± 0.3 for ACHN EV and 36.67 ± 5.7 for ACHN OIP5 (Figure 9A & 9B). The number of colonies produced by ACHN OIP5 is significantly higher than the colonies of ACHN EV. In addition, the diameter of the colonies for ACHN OIP5 is greater than ACHN EV at the same magnification (Figure 9C).

A)

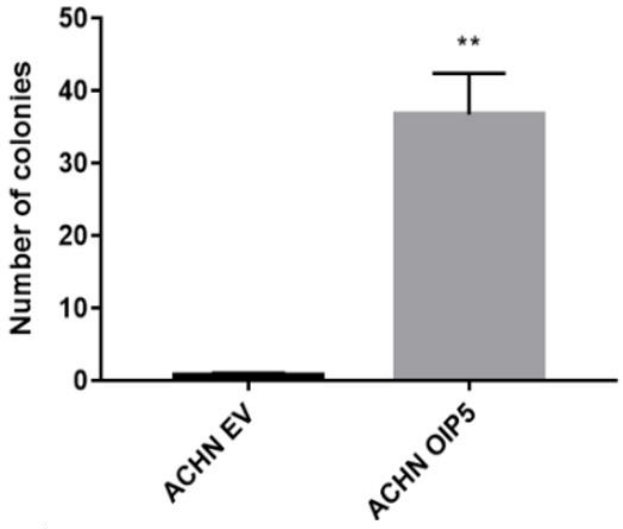

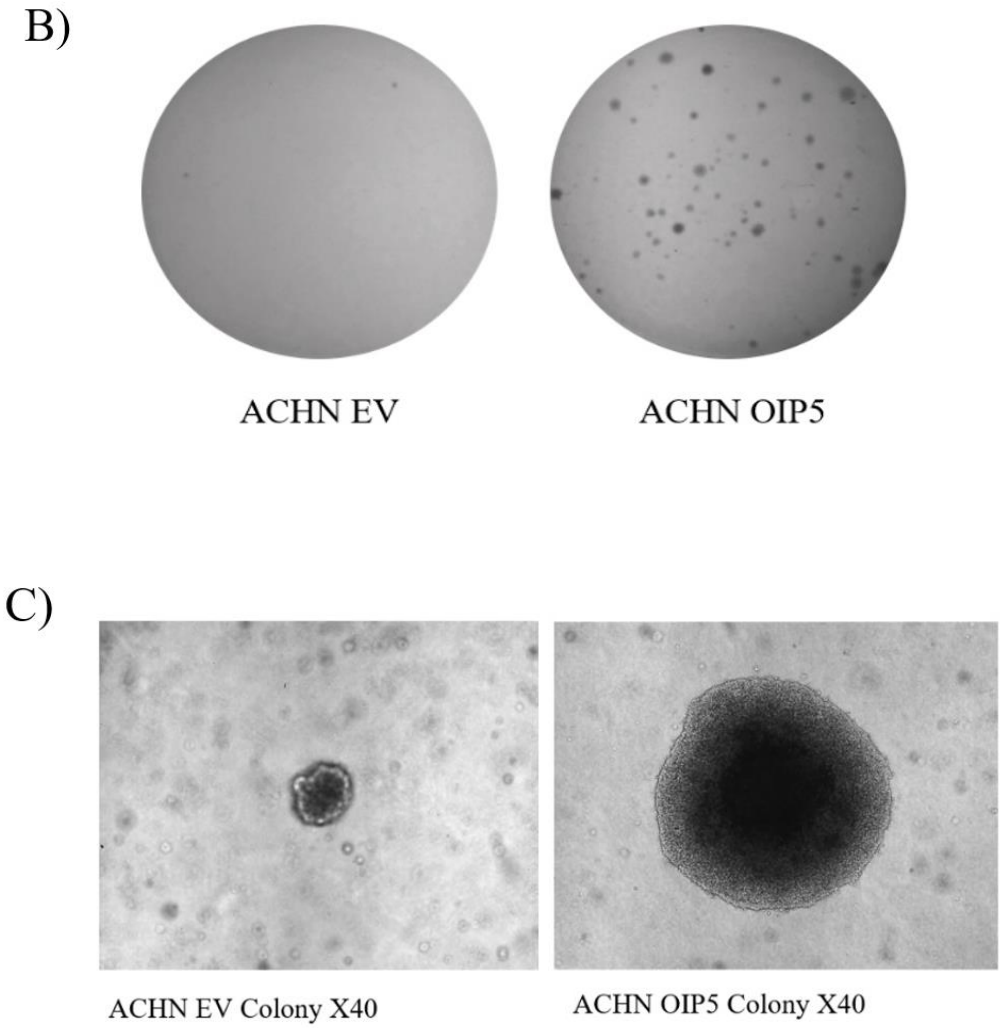

Figure 9. Soft agar colony formation assay for ACHN stable lines. Experiments were repeated three times. A) Soft agar colony formation assay for ACHN EV and ACHN OIP5 in 10^6 cells/well. B) Analysis of the soft agar colony formation assay for ACHN stable lines in 10^6 cells/well. C) ACHN EV colony formed in the soft agar at 40X magnification. D) ACHN OIP5 colony formed in the soft agar at 40X magnification. Experiments were repeated three times. Student t-test was conducted for the analysis. All data are presented as mean ± SE. * indicates significant different between ACHN OIP5 and ACHN EV, * when $p \leq 0.05$, ** when $p \leq 0.01$, *** when $p \leq 0.001$, **** when $p \leq 0.0001$.

4.2 OIP5-facilitaed enhancement of ACHN cell invasion

Besides *in vitro* analyses of cell's oncogenic properties via anchorage-dependent and -independent proliferation, the oncogenic potential can also be documented *in vitro* by cell's invasion capacity. Transwell invasion assay was thus performed on the ACHN stable lines (Figure 10). After 12-hr starvation and 24-hr incubation, the percentage of ACHN OIP5 cells passed through the membrane is 24%, which is higher than ACHN EV cells (16.7%) (Data not shown). When the starvation time and incubation time increased to 24hrs and 48hrs respectively, the percentage of ACHN OIP5 migrated through the Matrigel membrane elevated to an average of 89%± 0.2%, which is significantly higher than the average of its EV with 13.7% %± 0.2% migration (Figure 10). The increase of starvation and incubation time for ACHN significantly increases the ability for ACHN OIP5 to migrate through the matrigel membrane while this ability of ACHN EV stays similar.

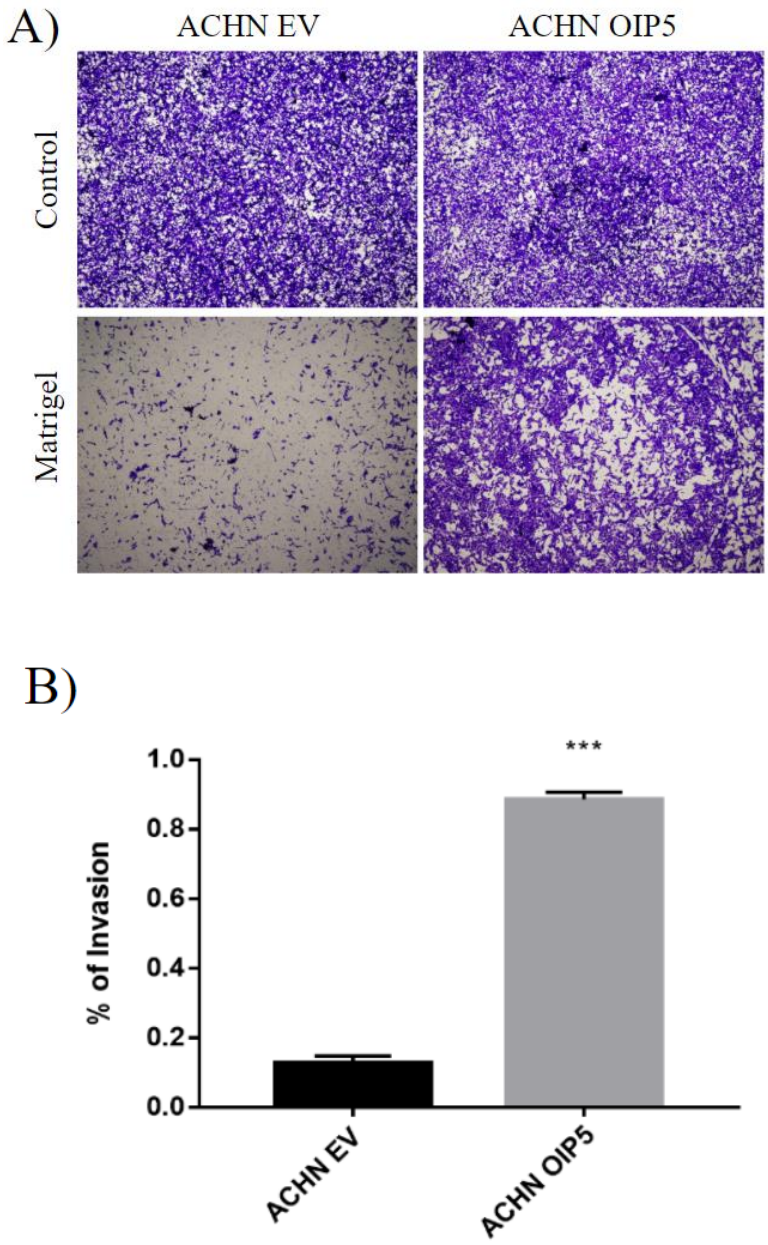

Figure 10. Transwell invasion assay of ACHN EV and ACHN OIP5. A) Transwell invasion assay of ACHN EV and ACHN OIP5 with 24hrs starvation. The cells that passed through the membranes were stained after 48hrs. B) The percentage of the cells that passed through the membrane compared to the control insert for ACHN stable lines with 24hrs starvation and 48hrs incubation. Experiments were repeated three times. Student t-test was conducted for the analysis. All data are presented as mean ± SE. * indicates significant different between ACHN OIP5 and ACHN EV, * when $p \leq 0.05$, ** when $p \leq 0.01$, *** when $p \leq 0.001$, **** when $p \leq 0.0001$.

4.3 OIP5-mediated enhancement of tumorigenesis

As the *in vitro* analyses above support the oncogenic role of OIP5 in pRCC ACHN cells, the ability of the stable lines to form xenografts in NOD-SCID mice with and without OIP5 ectopic expression were examined. The time to the endpoint of the mice bearing ACHN EV and ACHN OIP5 tumors was recorded to investigate the kinetics of tumorigenesis of the stable lines (Figure 11A). Survival time of the mice were analyzed and the mice with ACHN OIP5 xenograft had significantly lower survival compare to the mice implanted ACHN EV (Figure 11B). The average survival time of the of the mice with ACHN OIP5 implanted is 48.2 ± 1.96 days, while the average survival time of ACHN EV implanted mice is 59.6 ± 1.99 days respectively. Survival curve for the mice with ACHN OIP5/EV implanted were constructed and indicated in Figure 11C.

A)

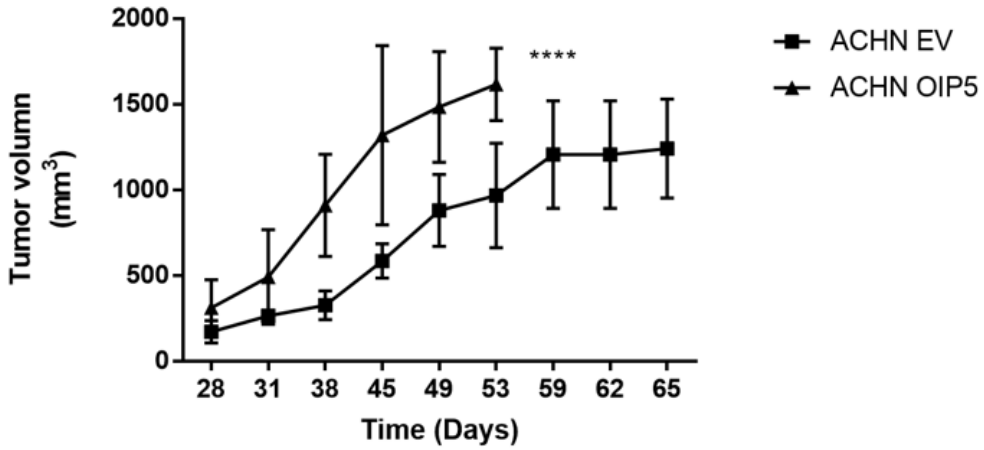

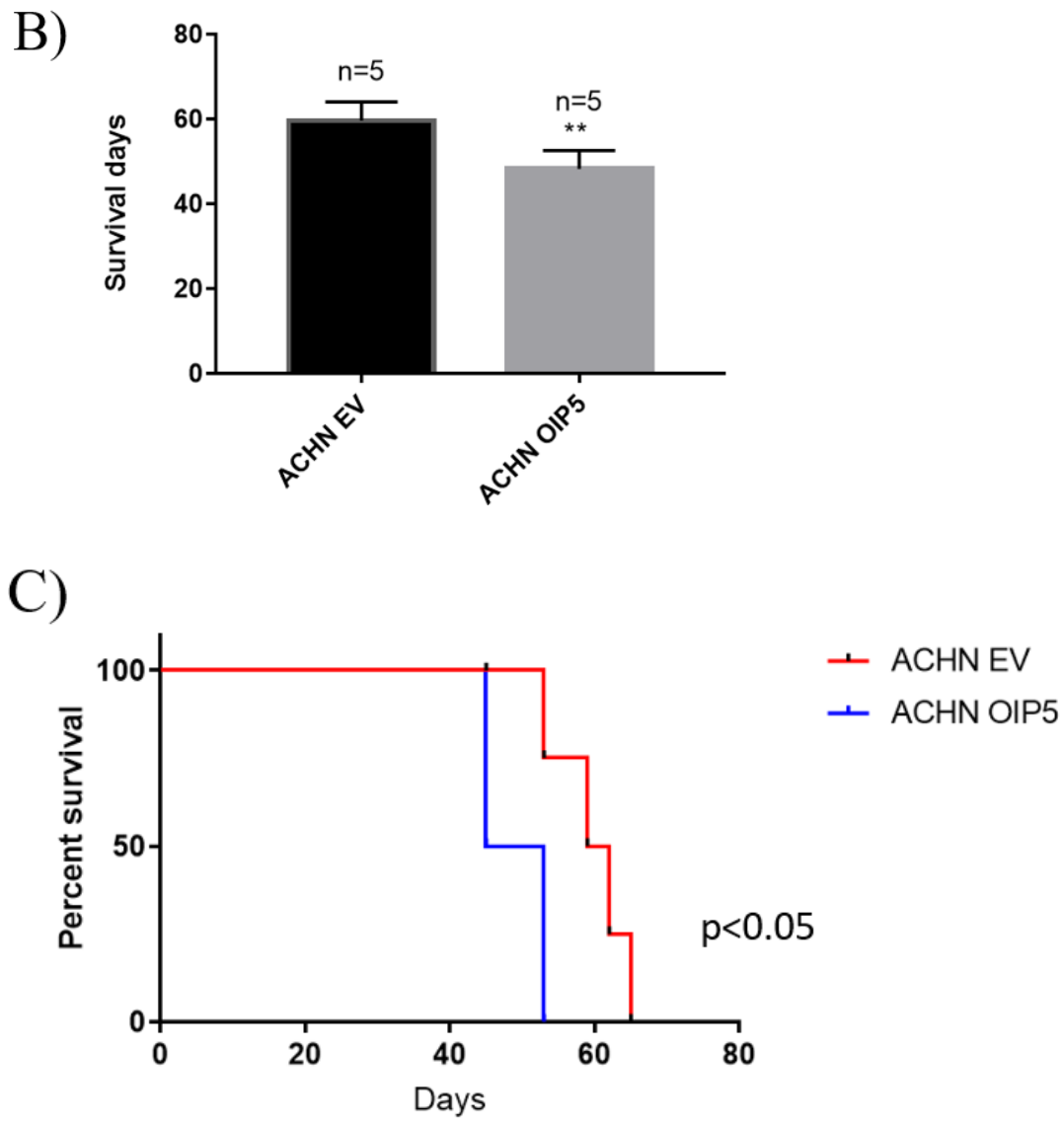

Figure 11. Xenograft tumor formation by ACHN stable lines. A) Tumor volume at different time points. B) Analysis of the survival length for the mice injected ACHN EV and ACHN OIP5. C) Survival curve of the mice with ACHN EV and ACHN OIP5 injection. Two-way ANOVA and Student t-test were conducted for the analysis. All data are presented as mean ± SE. * indicates significant different between ACHN OIP5 and ACHN EV, * when $p \leq 0.05$, ** when $p \leq 0.01$, *** when $p \leq 0.001$, **** when $p \leq 0.0001$.

The expression of OIP5 was examined by IHC to confirm the level of OIP5 in ACHN OIP5 and ACHN EV xenograft (Figure 12). There were 5 ACHN EV xenograft tumor and ACHN OIP5 xenograft tumor. OIP5 expression is significantly elevated in ACHN OIP5 xenograft compared to ACHN EV xenograft. The average stain intensity of ACHN OIP5 and ACHN EV xenografts are 123.9 ± 9.829 and 62.33 ± 10.51 respectively.

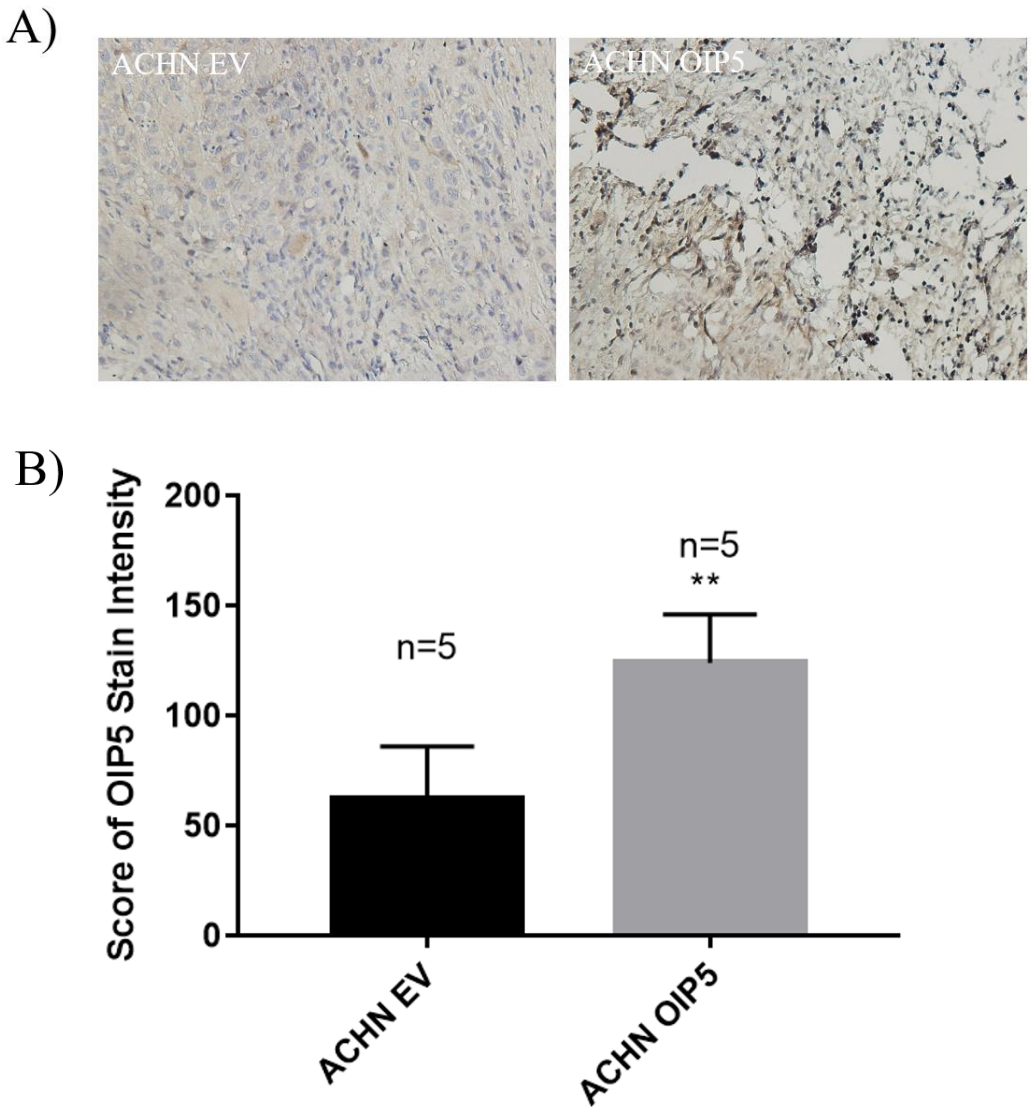

Figure 12. IHC staining and statistical analysis of OIP5 expression for ACHN EV and ACHN OIP5 xenograft tumors. A) Image of IHC staining for ACHN OIP5 and EV xenograft tumor. B) Statistical analysis of OIP5 expression for ACHN EV and ACHN OIP5 xenograft tumors. Student t-test was conducted for the analysis. All data are presented as mean ± SE. * indicates significant different between ACHN OIP5 and ACHN EV, * when $p \leq 0.05$, ** when $p \leq 0.01$, *** when $p \leq 0.001$, **** when $p \leq 0.0001$.

4.4 CDK2, H3 and Ki67 expressions in the xenografts

The elevations of ACHN OIP5 cell proliferation in vitro (see section 4.1 for details) suggest a higher level of cell proliferation in ACHN OIP5 cell-derived xenograft tumors than the xenograft tumors produced by ACHN EV cells. In line with this notion, upregulation of CDK2 was observed in ACHN OIP5 xenografts compared to ACHN EV tumors (Figure 13). The intensity of OIP5 staining in ACHN OIP5 and ACHN EV tumors is 81.36 ± 13.220 and 11.44 ± 5.049 respectively.

To further validate the concept, Histone H3 phosphorylation at serine 10(S10), which is a typical event occurred in M phase, was examined (Hans and Dimitrov, 2001 (Figure 14). The average stain intensity of ACHN OIP5 xenograft tumor is higher than ACHN EV xenograft tumor, while the differences did not reach to a significant level at $p < 0.05$. Histone H3 phosphorylation levels of ACHN OIP5 and ACHN EV are 103.2 ± 18.74 and 74.43 ± 17.02 respectively.

Since the data related to Histone H3 S10 phosphorylation is not conclusive, Ki67 status in both ACHN EV and ACHN OIP5 xenografts were investigated (Figure 15). There was no significant difference for the expression of Ki67 between ACHN OIP5 and EV xenograft tumors, even Ki67 expression level is elevated in ACHN OIP5 xenografts compared to ACHN EV xenografts. The expression level of Ki67 for ACHN OIP5 and ACHN EV xenograft are 127.4 ± 12.28 and 115.5 ± 5.534 respectively.

A)

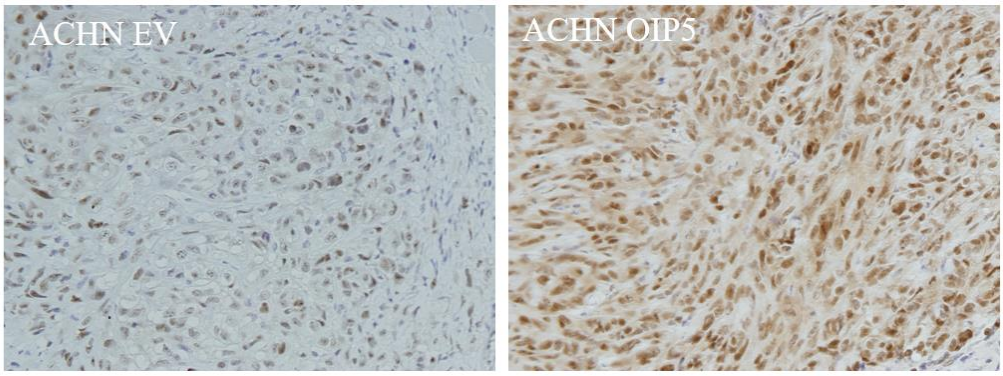

B)

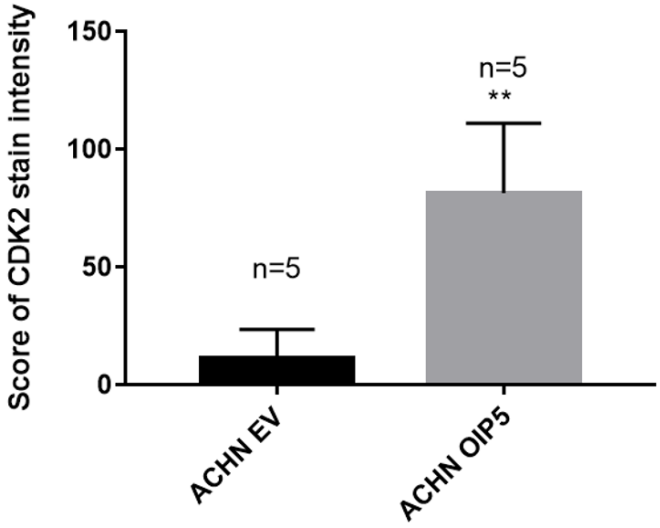

Figure 13. IHC staining and statistical analysis of CDK2 expression for ACHN EV and ACHN OIP5 xenograft tumor. A) Image of IHC staining for ACHN OIP5 and EV xenograft tumor. B) Statistical analysis of CDK2 expression for ACHN EV and ACHN OIP5 xenograft tumors. Student t-test was conducted for the analysis. All data are presented as mean ± SE. * indicates significant different between ACHN OIP5 and ACHN EV, * when $p \leq 0.05$, ** when $p \leq 0.01$, *** when $p \leq 0.001$, **** when $p \leq 0.0001$.

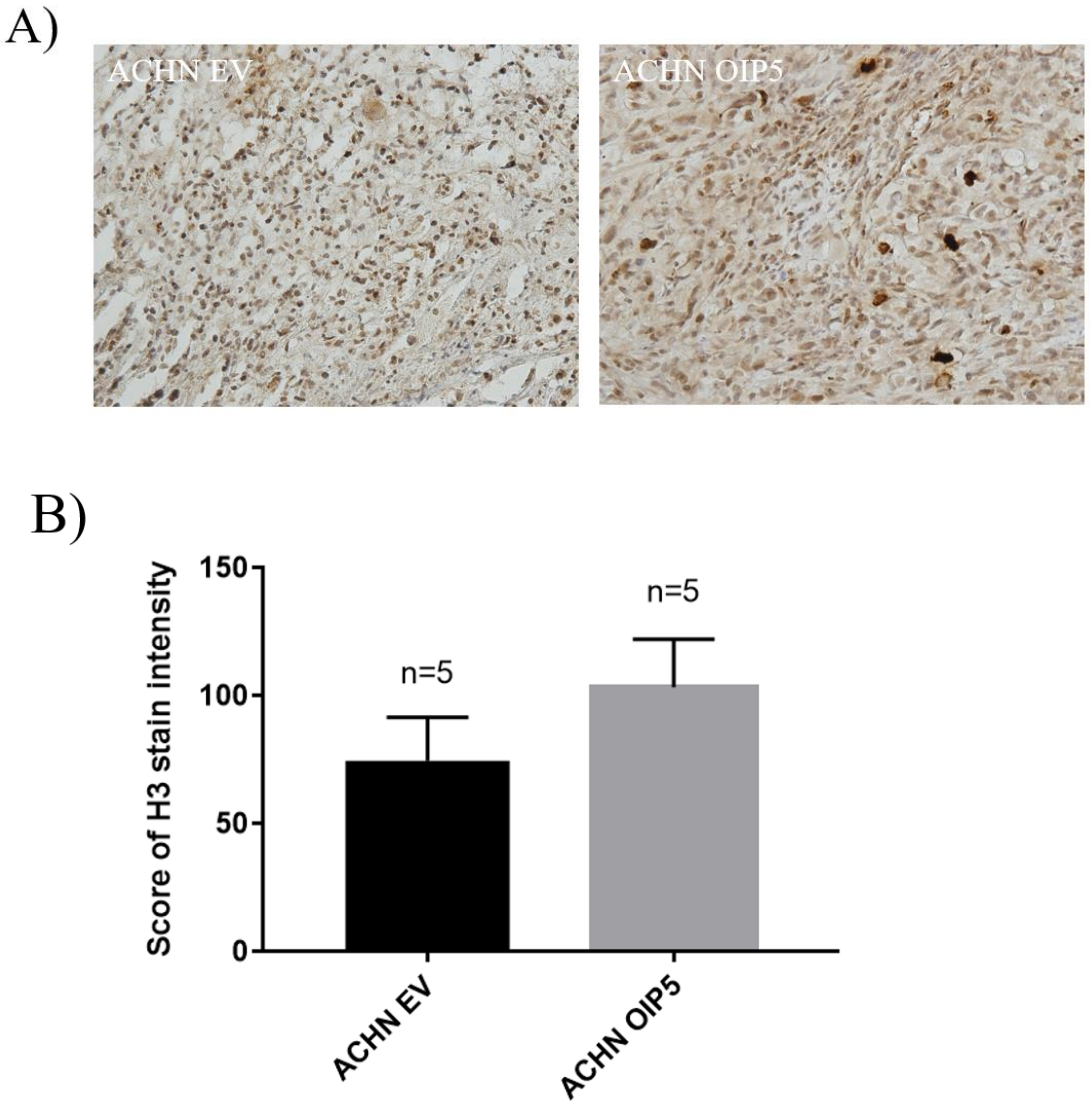

Figure 14. IHC staining and statistical analysis of H3 S10 phosphorylation level for ACHN EV and ACHN OIP5 xenograft tumor. A) Image of IHC staining for ACHN OIP5 and EV xenograft tumor. B) Statistical analysis of H3 phosphorylation for ACHN EV and ACHN OIP5 xenograft tumors. Student t-test was conducted for the analysis. IHC staining intensity of ACHN OIP5 is not significantly higher than ACHN EV. All data are presented as mean ± SE.

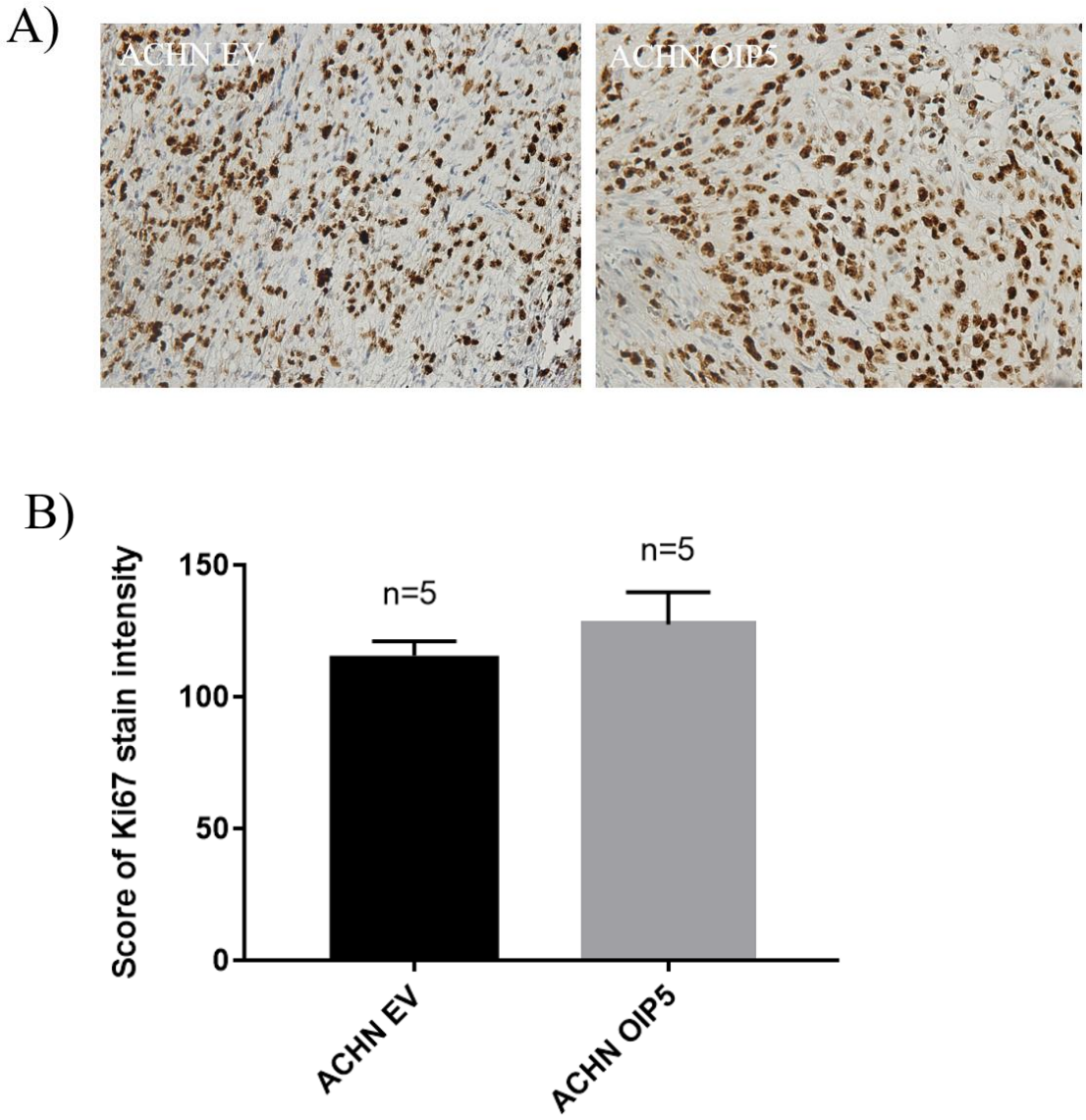

Figure 15. IHC staining and statistical analysis of Ki67 for ACHN EV and ACHN OIP5 xenograft tumor. A) Image of IHC staining for ACHN OIP5 and EV xenograft tumor. B) Statistical analysis of Ki67 for ACHN EV and ACHN OIP5 xenograft tumors. Student t-test was conducted for the analysis. IHC staining intensity of ACHN OIP5 is not significantly higher than ACHN EV. All data are presented as mean ± SE.

4.5 RNA expression of PLK1 and CDK1 is elevated with OIP5 overexpression

OIP5 plays a critical role in kinetochore formation at the late M and early G1 phase which may be affected by a set of factors including CENP-1, AURKB, PLK1, CDK1, CCNB2 and BUB1 with possible alterations of their expression in ACHN OIP5 xenografts compare to ACHN EV xenografts. RT-PCR was performed for the RNA expression of CENP-A, AURKB, PLK1, CCNB2, CDK1, and BUB1 in ACHN OIP5 and ACHN EV xenograft tumors (Figure 16). Among all of RNA expression examined, the RNA expressions of PLK1 and CDK1 in ACHN OIP5 xenograft tumor are significantly increased compares to ACHN EV tumors. The average RNA expressions of CENP-A, AURKB, and BUB1 in ACHN EV is higher than ACHN OIP5 while the difference is not significant. The average RNA fold change of CENP-A, AURKB, PLK1, CCNB2, CDK1, and BUB1 are 0.803 ± 0.1531, 1.055 ± 0.087, 1.032 ± 0.073, 0.8317 ± 0.050, 1.018 ± 0.087, and 1.026 ± 0.174 for ACHN EV, 0.6162 ± 0.1424, 0.9276 ± 0.1068, 1.465 ± 0.08871, 0.8334 ± 0.0421, 1.6 ± 0.2139, and 0.9717 ± 0.1339 for ACHN OIP5 respectively. Collectively, the detection of increases in CDK1 and PLK1 expression supports the involvement of both proteins in the kinetochore assembly in ACHN OIP5 tumors.

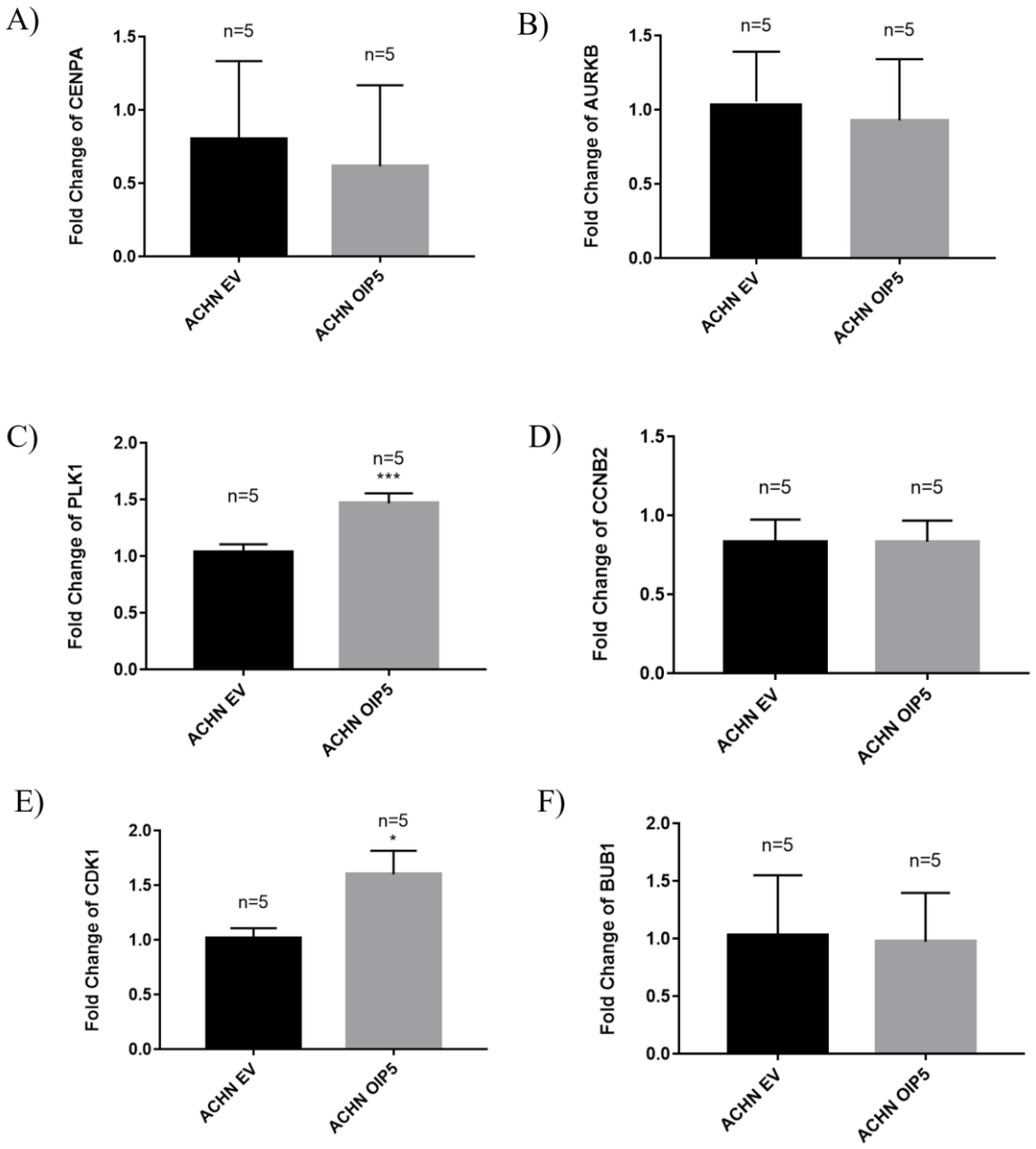

Figure 16. RT-PCR of ACHN EV and ACHN OIP5 xenograft. A) Statistical analysis for the RNA expression of CENP-A in ACHN EV and ACHN OIP5. Experiments were repeated three times. B) Statistical analysis for the RNA expression of AURKB in ACHN EV and ACHN OIP5. C) Statistical analysis for the RNA expression of PLK1 in ACHN EV and ACHN OIP5. D) Statistical analysis for the RNA expression of CCNB2 in ACHN EV and ACHN OIP5. E) Statistical analysis for the RNA expression of CDK1 in ACHN EV and ACHN OIP5. F) Statistical analysis for the RNA expression of BUB1 in ACHN EV and ACHN OIP5. Student t-test was conducted for the analysis. All data are presented as mean ± SE. * indicates significant different between ACHN OIP5 and ACHN EV, * when $p \leq 0.05$, ** when $p \leq 0.01$, *** when $p \leq 0.001$, **** when $p \leq 0.0001$.

4.6 PLK1 inhibitor leads to G2/M phase arrest for ACHN OIP5 stable cells

Since PLK1 plays a key role in chromatin segregation (Schmucker and Sumara, 2014), its elevation in ACHN OIP5 cell-derived xenografts may plays a major role in cell cycle progression. Therefore, cell cycle distribution in ACHN EV and ACHN OIP5 cells were conducted to test such possibility. Cell cycle distribution analysis demonstrated that the overexpression of OIP5 in ACHN cells has no significant influence on the cell cycle of ACHN (Figure 17 & Table 2). The average percentages of cells in G1 phase and G2/M are 46.8% and 31.1% for ACHN EV, 44.9% and 33.6% for ACHN OIP5 respectively. There are less ACHN OIP5 cells in G1 phase and more cells in G2/M phase when compared to ACHN EV, however, the difference was not significant.

Next, cell cycle profiles with inhibited PLK1 activity in ACHN EV and ACHN OIP5 cells were performed. Cell cycle analysis was conducted for ACHN OIP5 and ACHN EV stable lines with PLK1 inhibitor (40nM) treated for 72 hrs (Figure 18 & Table 3). ACHN OIP5 stable line has significantly more cells arrested at G2/M phase than ACHN EV stable lines while ACHN EV stable line has significantly more cells in G1 phase. The average percentage of ACHN OIP5 and ACHN EV cells are 20.8% ± 0.7 and 40.43% ± 2.09 for G1 phase, 48.7% ± 0.29 and 31.67% ± 1.34 for G2/M phase respectively. These observations strongly suggest a dependence of ACHN OIP5 cell on PLK activities to progress through M phase which is consistent with the critical roles of PLK in M phase progression.

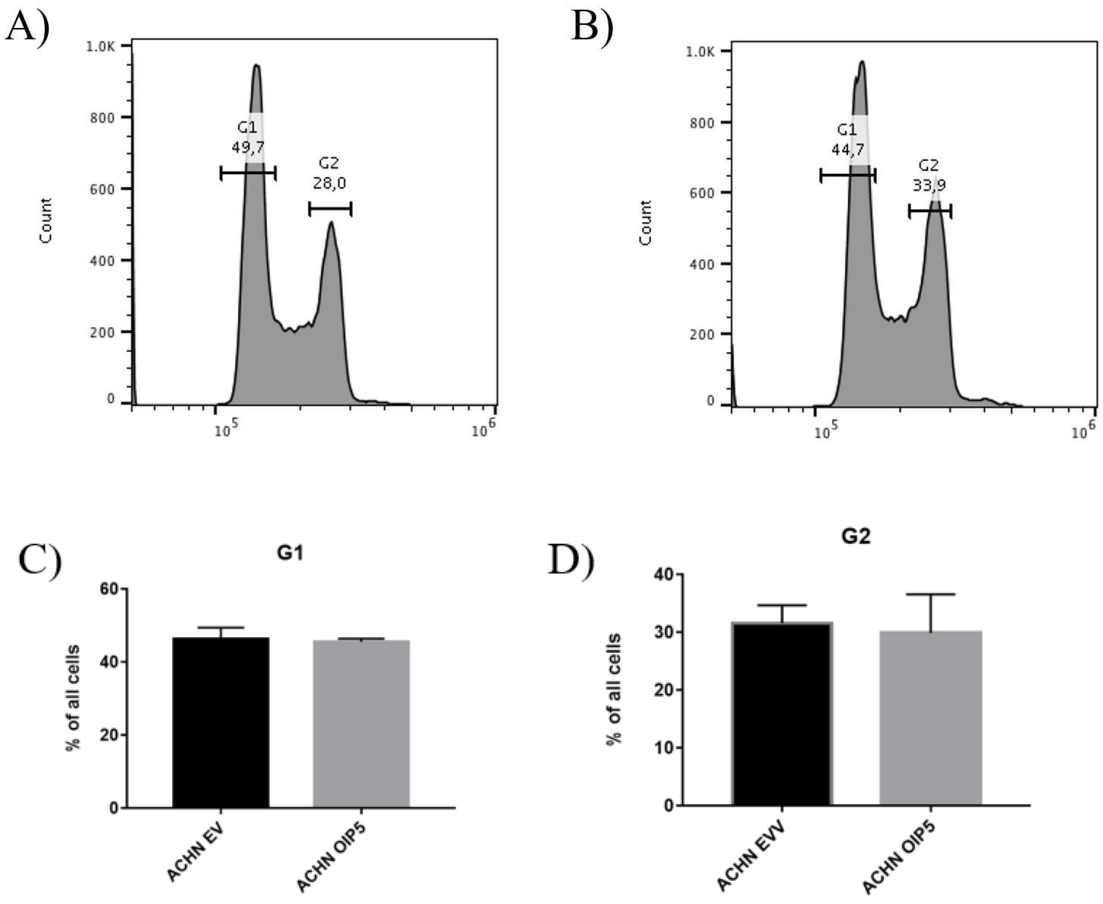

Figure 17. Cell cycle distribution analysis of ACHN EV and ACHN OIP5 stable lines. Experiments were repeated three times. A) Cell cycle distribution of ACHN EV. B) Cell cycle distribution of ACHN OIP5. Experiments were repeated three times. C) Statistical analysis for the percentage of ACHN EV and ACHN OIP5 in G1 phase. D) Statistical analysis for the percentage of ACHN EV and ACHN OIP5 in G2 phase. Student t-test was conducted for the analysis. All data are presented as mean ± SE. No significance is found. All data are presented as mean ± SE.

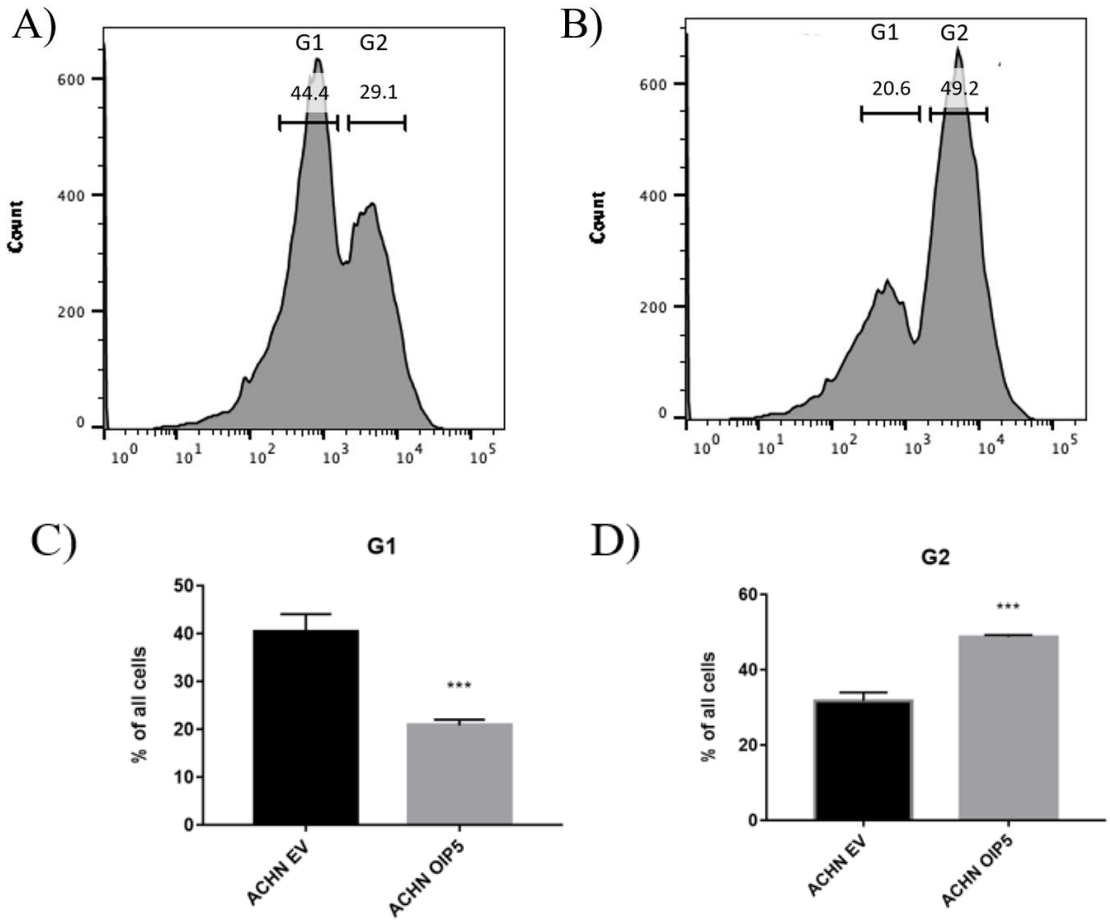

Figure 18. Cell cycle distribution analysis of PLK1 inhibitor (BI 2536, 72hr, 40nM) treated ACHN EV and ACHN OIP5 stable lines. Experiments were repeated three times. A) Cell cycle distribution analysis of PLK1 inhibitor treated ACHN EV. B) Cell cycle distribution analysis of PLK1 inhibitor treated ACHN OIP5. C) Statistical analysis for the percentage of PLK1 inhibitor treated ACHN EV and ACHN OIP5 in G1 phase. D) Statistical analysis for the percentage of PLK1 inhibitor treated ACHN EV and ACHN OIP5 in G2 phase. Student t-test was conducted for the analysis. All data are presented as mean ± SE.* indicates significant different between ACHN OIP5 and ACHN EV, * when $p \leq 0.05$, ** when $p \leq 0.01$, *** when $p \leq 0.001$, **** when $p \leq 0.0001$.

Table 2. Average percentage of ACHN EV and ACHN OIP5 in G1 and G2/M phase

	G1	G2/M
ACHN EV	46.83±2.48	27.80±5.60
ACHN OIP5	44.93±1.37	33.60±0.26

Table 3. Average percentage of PLK1 inhibitor treated ACHN EV and ACHN OIP5 in G1 and G2/M phase

	G1	G2/M
ACHN EV	40.43±2.09	31.67±1.34
ACHN OIP5	20.80±0.70***	48.70±0.29***

4.7 Upregulation of OIP5 in ccRCC and pRCC

The expression of OIP5 was examined on a tissue microarray (TMA) with both ccRCC and pRCC tissues, together with their tissues adjacent to the cancer tissues (AT tissue) (Table 4). There were a total of 37 ccRCC patients with each patient contributed 4 tissues, including 2 cancer tissues and 2 AT tissues, resulting in 73 ccRCC tissues and the same number of the correlated AT tissues (1 ccRCC grade 1 tissue was missed during processing, therefore, its correlated AT tissues was not included). These ccRCCs consist of grade 1 (n=25), grade 2 (n=10), and grade 3 (n=2) tumors (Table 5); these tissues were immunohistochemistry (IHC) stained for OIP5 (Figure 19). In order to elucidate the data, ccRCC tissues and the corelated AT tissues were separated into two groups, ccRCC grade 1 and ccRCC grade 2&3. The expression of OIP5 is significantly higher in the RCC tissues with high grade (Grade 2&3) compared to their matched AT non-tumor tissues and grade 1 ccRCC tissues (Figure 19B), suggesting that OIP5 upregulation is associated with ccRCC progression The average stain intensity of ccRCC grade 1, ccRCC grade 2&3, grade 1 ccRCC AT and grade 2&3 AT are 25.78± 2.71, 74.56± 4.95, 22.09±3.05 and 36.08± 3.75 respectively.

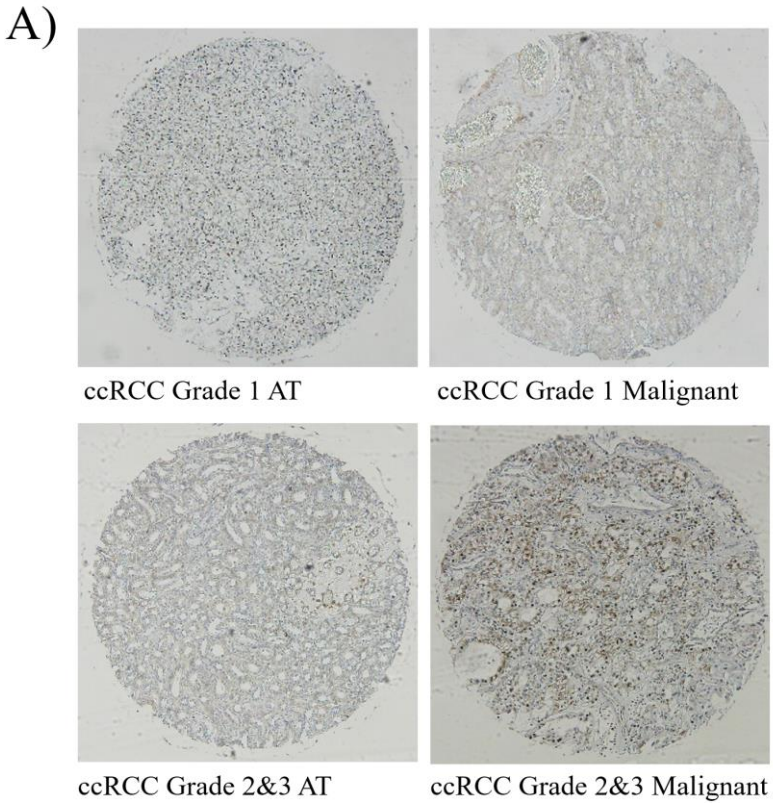

Figure 19. IHC staining and statistical analysis for ccRCC TMA. A) Image of IHC staining for ccRCC tissues. B) Statistical analysis of OIP5 expression for ccRCC tissues and ccRCC AT tissues. One-way ANOVE and Student t-test were conducted for the analysis. All data are presented as mean ± SE. * indicates significant different between ACHN OIP5 and ACHN EV, * when $p \leq 0.05$, ** when $p \leq 0.01$, *** when $p \leq 0.001$, **** when $p \leq 0.0001$.

In addition to the expression of OIP5 in ccRCC tissues, the expression of OIP5 was also examined in pRCC tissues, together with their tissues adjacent to the cancer tissues (AT tissue). There was a total of 20 pRCC patients (Table 4) with each patient contributed 4 tissues, including 2 cancer tissues and 2 AT tissues, resulting in 40 pRCC tissues and the same number of the correlated AT tissues. pRCC tissues contain stage 1 (n=13), stage 2 (n=4), and stage 3 (n=3) tumors (Table 6) and are separated into T1 and T2&3 based on their disease stages. The expression of OIP5 in both pRCC T1 and pRCC T2&3 are significantly higher than their correlated AT tissues (Figure 20B). Moreover, the expression of OIP5 in pRCC T2&3 is significantly higher than the expression of OIP5 in pRCC T1 (Figure 20B). The average stain intensity of pRCC T1, pRCC T2&3, pRCC T1 AT and pRCC T2&3 AT are 46.03± 4.84, 74.95± 6.16, 8.02±0.82 and 9.18±1.1 respectively.

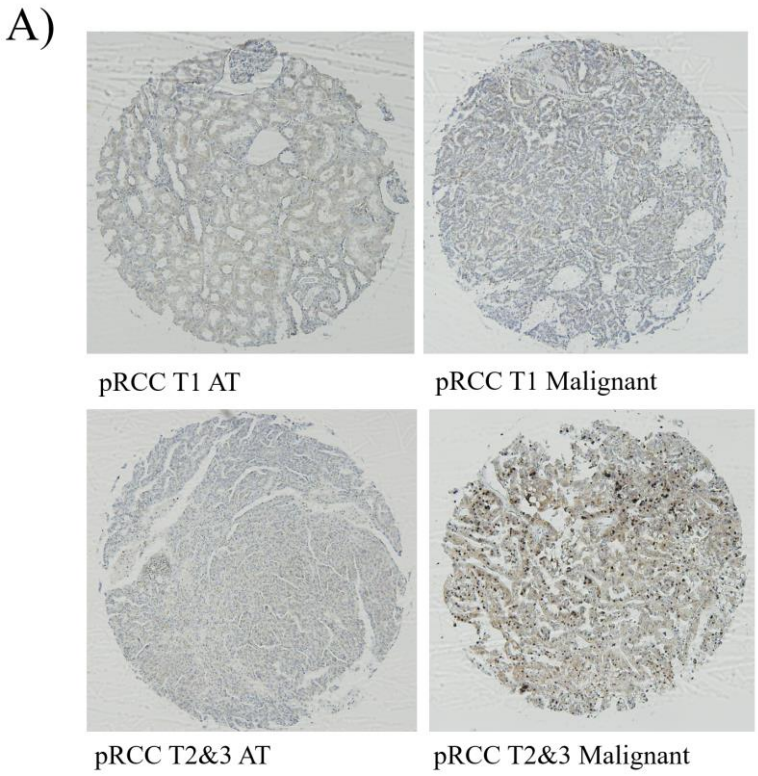

Figure 20. IHC staining and statistical analysis for pRCC TMA. A) Image of IHC staining for pRCC tissues. B) Statistical analysis of OIP5 expression for pRCC tissues and pRCC AT tissues. One-way ANOVE and Student t-test were conducted for the analysis. All data are presented as mean ± SE. * indicates significant different between ACHN OIP5 and ACHN EV, * when $p \leq 0.05$, ** when $p \leq 0.01$, *** when $p \leq 0.001$, **** when $p \leq 0.0001$.

Table 4. Summary of pathology data of TMA

Pathology	Number of tissue cores
Cancer adjacent kidney tissue (Clear cell carcinoma)	37
Cancer adjacent kidney tissue (Papillary renal cell carcinoma)	20
Clear cell carcinoma	37
Papillary renal cell carcinoma	20

Table 5. ccRCC tumor grade data of TMA

Tumor Grade	Number of tissue cores
Grade 1	25
Grade 2	10
Grade 3	2

Table 6. pRCC tumor stage data of TMA

Tumor Stage	Number of tissue cores
Stage 1 (T1)	13
Stage 2 (T2)	4
Stage 3 (T3)	3

4.8 Association of OIP5 mRNA expression with poor survival of ccRCC and pRCC patients

With the above demonstrations of OIP5 increases in RCCs, we analyzed a potential association of OIP5 upregulation with overall survival. RNA expression data was downloaded and analyzed from Kaplan-Merier plotter (www.kmplot.com). Both ccRCC and pRCC within the group marked with high OIP5 expression have poor 5-year and long-term overall survival (Figure 21). Collectively, OIP5 mRNA expression can significantly stratify the fatality risk of ccRCC and pRCC; this knowledge can be explored for clinical assessment of ccRCC and pRCC prognosis.

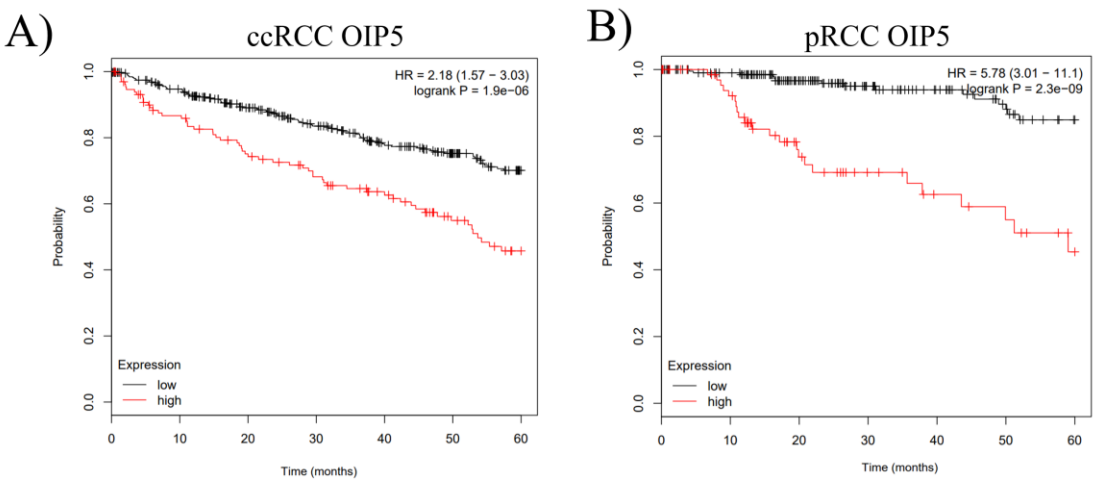

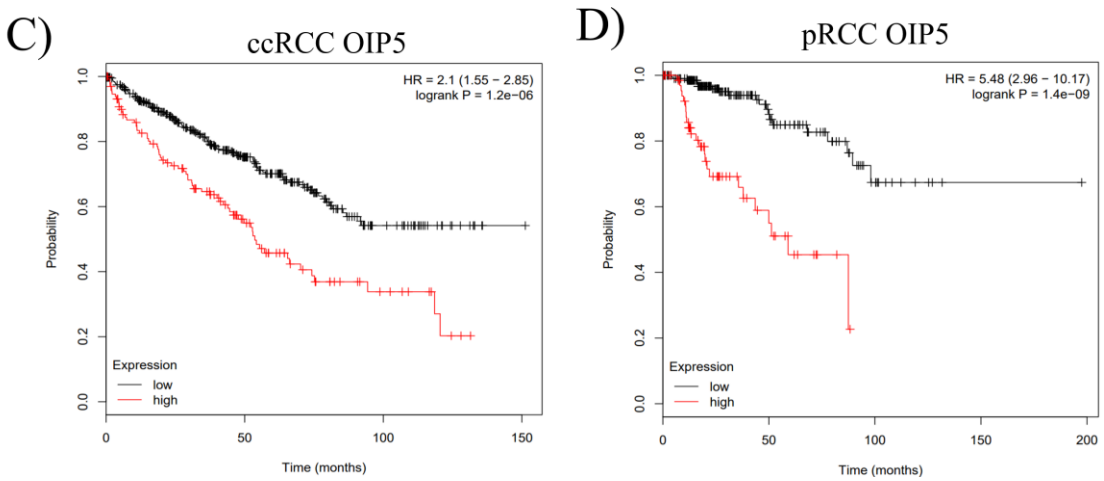

Figure 21. Kaplan-Meier plots for the overall survival curve of RCC patients with high OIP5 expression and low OIP5 expression. A) Five-year survival curve of ccRCC patients with high OIP5 expression and low OIP5 expression. B) Five-year survival curve of pRCC patients with high OIP5 expression and low OIP5 expression. C) Long-term survival curve of ccRCC patients with high OIP5 expression and low OIP5 expression. D) Long-term survival curve of pRCC patients with high OIP5 expression and low OIP5 expression.

Data was retrieved from: www.kmplot.com

V. DISCUSSION

Extensive research has demonstrated that OIP5 is upregulated in several cancers, including kidney, gastric, colorectal, lung and esophageal cancer (Li *et al*, 2018). OIP5 is a testis-specific protein and its expression in other organs is normally low, suggesting its potential as a biomarker and therapeutic target for various cancers (Zhang *et al*, 2017). RCC contributes to approximately 3% of all human cancers, and it is the most common type of kidney malignancy (Hsieh *et al*, 2017). It is a heterogeneous disease with multiple subtypes, but diagnosis methods and treatments for different RCC remain limited (Hsieh *et al*, 2017). Therefore, promising biomarkers and therapeutic targets for RCC is in demand. This study reveals that OIP5 contributes to pRCC and that OIP5 expression possesses biomarker and therapeutic potential for ccRCC and pRCC.

Cell experiments with overexpression of OIP5 have indicated that OIP5 promotes ACHN cell proliferation and colony formation. Abnormal elevations of cell proliferation are a typical feature of cancer, evident by the common alteration of proteins regulating cell cycle progression in cancer cells (Feitelson *et al*, 2015). The growth of normal tissues is strictly regulated by cell signaling, while such control is disrupted in cancer (Feitelson *et al*, 2015). The OIP5-mediated promotion of ACHN pRCC cell proliferation is thus in accordance with this knowledge. However, ectopic OIP5 expression has no effects on the proliferation of A498 and 786-O cells. The underlying mechanisms for the differential impact of OIP5 on pRCC and ccRCC cell proliferation might be complex. The lower level of ectopic OIP5 expression in both A498 and 786-0 cells compared to ACHN pRCC cells (Figure 4) might be an attribute. It is also possible that the intrinsic cellular signaling network of ccRCC cells might

attenuate OIP5 activity in enhancing ccRCC cell proliferation; this attenuation might be in part via regulating the level of OIP5 protein. However, the impact of OIP5 on ccRCC and pRCC cell proliferation should also be investigated through knockdown or knockout of endogenous OIP5. Despite several attempts, we were unable to knockdown of OIP5 in ACHN cells, which indirectly supports an essential role of OIP5 in ACHN cell proliferation. It will be interesting to examine the impact of downregulation of endogenous OIP5 on the proliferation of ccRCC cells in future.

Previous studies have revealed that OIP5 interacts with multiple oncogenic proteins in RAF-MEK-MEK and PI3K-AKT-mTOR pathway, resulting in the enhancement of cell growth, proliferation, angiogenesis and suppression of cell apoptosis (Fouad and Aanei, 2017). Whether these molecular events contribute to OIP5-mediated promotion of ACHN cell proliferation should be investigated in future.

Beside increases in ACHN cell's proliferation ability, OIP5 also renders the cells more invasive, an essential property underlying cancer metastasis (Justus *et al*, 2014). Metastatic cancers are lethal, and it is the primary cause of cancer related death (Qian *et al*, 2017). The development of metastasis is a multiple-step process involving epithelial-mesenchymal transition (EMT), which cancer cells lost their adhesion and invade extracellular matrix to intravasate into blood stream or lymph system (Banyard and Bielenberg, 2016). The cancer cells then will be carried to distant organs, extravasate from the vessels and re-establish tumor at the new foci, completing mesenchymal-epithelial transition (MET) (Banyard and Bielenberg, 2016). Whether EMT is a mechanism governing OIP5-stimulated ACHN cell invasion is an intriguing question that needs to be addressed in future.

The *in vitro* observations of OIP5 in stimulating ACHN pRCC cell's oncogenic properties are further supported by OIP5's activities in promoting ACHN cell to form tumors in NOD-SCID mice. Formation of xenograft *in vivo* is likely more complex compared to *in vitro* analyses of cell's ability in proliferation, anchorage-independent growth, and invasion. Whether any of these *in vitro* events stimulated by OIP5 makes a major contribution to OIP5-derived enhancement of xenograft formation remains to be determined. Despite these uncertainties, it is tempting to speculate OIP5-promoted ACHN cell proliferation might not be the whole story for the enhanced ACHN cell xenograft tumors since ACHN OIP5 cell-produced xenograft tumors do not express significantly higher levels of H3 S10 phosphorylation and Ki67 compared to ACHN EV cell-derived tumors. However, this does not exclude the possibility that ACHN OIP5 tumors rely more on OIP5 for tumor cell proliferation compared to the ACHN EV xenografts.

This possibility is supported by elevations of cyclin dependent kinase 2 (CDK2) in ACHN OIP5 tumors. CDK2 belongs to the cyclin-depend kinase family of Ser/Thr protein kinase (Peng *et al*, 2016). The transcriptional activity of E2F transcription factor (E2Fs) is inhibited by retinoblastoma (Rb) in G0 phase (Tadesse *et al*, 2019). When entering G1 phase, Rb protein is partially phosphorylated by cyclin D bonded CDK4 and/or CDK6, resulting in the activation of E2Fs and the production of CDK2 which forms complex with cyclin E (Peng *et al*, 2016). Rb is further phosphorylated by CDK2-cyclin E complex, leading to the release of E2Fs and trigger the transcription of the proteins that are necessary for S phase such as cyclin A (Tadesse *et al*, 2019). CDK2 continues to contribute itself by binding with cyclin A to maintain the phosphorylation

of Rb and monitor cell cycle progression (Tadesse *et al*, 2019). CDK2 is an essential protein for cell cycle progression, and accumulated evidence showed the upregulation of CDK2 leads to abnormal cell proliferation in cancers (Chohan *et al*, 2015). In addition, study performed by Hongo *et al* demonstrated that high CDK2 specific activity is associated with poor prognosis and low recurrence free survival rate in RCC (Hongo *et al*, 2014). According to CDK2 IHC staining of this study, the expression of CDK2 in ACHN OIP5 xenograft is upregulated compared to ACHN EV xenograft, suggesting overexpression of OIP5 results in elevated expression of CDK2, which may associate with poor prognosis and low recurrence free survival rate in pRCC. However, we like to emphasize that this possibility certainly needs additional investigations, in part because we were unable to demonstrate upregulation of CDK2 activators (cyclin A and E) in ACHN OIP5 xenografts.

Intriguingly, we detected CDK1 increases in ACHN OIP5 xenografts. CDK1 is a highly conserved kinase and plays essential role in cell cycle regulation during the transition from G2 phase to mitosis (Prevo *et al*, 2018). In late G2 phase when the level of cyclin B is high enough to form stable complex with CDK1, cdc25 phosphatase removes the phosphorylation site of CDK1 and activates CDK1/cyclin B complex, resulting the activation of several transcriptional factors that participate in nuclear envelop breakdown, chromatin condensation, and spindle assembly (Prevo *et al*, 2018). Overexpression of CDK1 and cyclin B is associated with poor prognosis of breast, colorectal and lung cancer, while clinical evidence showed that targeting CDK1 can sensitize tumor cell, making CDK1 to be a potential therapeutic target (Prevo *et al*, 2018). CCNB2 belongs to B-type cyclins, and it is a critical protein in regulating G2-M

phase transition (Schubbar *et al,* 2013). Overexpression of CCNB2 is detected to provide proliferative advantage in several human tumors including lung, colorectal, breast and pituitary cancer (Schubbar *et al,* 2013). We need to be cautious in interpreting CDK1 upregulation in ACHN OIP5 xenografts, as we cannot show concurrent cyclin B upregulation.

The upregulation of PLK1 in ACHN OIP5 xenografts supports the relevance of cell proliferation in OIP5-enhanced ACHN cell tumor formation. PLK1 is a kinase which is required throughout mitosis by controlling bipolar spindle assembly during prometaphase, and support kinetochore-microtubule attachment (Schmucker and Sumara, 2014). Deposition of CENP-A is regulated by PLK1 in a Mis18 complex-dependent manner, as well as the protein stability of OIP5 and the maintenance of Mis18 complex localization (McKinley and Cheeseman, 2015). PLK1 is also known as a proto-oncogenic protein and its overexpression is found in lung, bladder and kidney cancer (Carcer, 2019). The upregulation of PLK1 in ACHN OIP5 xenografts suggests a major role of PLK1 in mediating M phase progression in these tumors. This possibility is supported by the dependence of ACHN OIP5 cells on PLIK1 for M phase progression *in vitro*. It is thus very intriguing to examine this possibility *in vivo*, i.e. whether the PLK1 inhibitor will be preferentially inhibit ACKN OIP5 xenograft tumor formation compared to ACHN EV cell-produced xenografts.

Confirmation of the above notion is highly clinically relevant as the upregulation of OIP5 occurs in primary pRCC is proved by our IHC examination of a RCC TMA. Furthermore, OIP5 upregulation is associated with poor overall survival of pRCC, an observation that strongly supports an important contribution of OIP5 in pRCC

progression. With this knowledge, the ability of PLK1 inhibitor in inhibiting the progression of pRCC expressing high levels of OIP5, should this be demonstrated, will bring a major benefit to patients having such aggressive pRCC. Collectively, our pioneer study reported here has a great potential for further exploration of OIP5 for its contributions to pRCC progression, its biomarker potential in assessing the fatality risk of pRCC, and its therapeutic applications.

VI. FUTURE DIRECTION

Since the evidence of this study indicates that overexpression of OIP5 promotes tumorigenesis both *in vitro* and *in vivo*, the next step of the study will be constructing xenograft by ACHN cell with both OIP5 overexpression and bioluminescence to monitor the dynamic of tumor growth; renal capsule injection will be the main technique utilized for tumorigenesis. Besides, the study will further examine therapeutic target potential of PLK1 inhibitor on ACHN stable lines. Moreover, study will continue examining the influence of OIP5 overexpression on A498 and 786O. Last but not least, study on the downstream proteins of OIP5 is necessary to further elucidate the mechanisms and pathways associated with OIP5.

VI. REFERENCES

Allshire, R. C., Karpen, G. H. (2008) Epigenetic regulation of centromeric chromatin: old dogs, new tricks? *Nat Rev Genet*. **9**, 923-937

Banyard, J., Bielenberg, D. R. (2016) The role of EMT and MET in cancer dissemination. *Connect Tissue Res*. **56**, 403-413

Barnhart, M. C., Kuich, P. H., Stellfox, M. E., Ward, J. A., Bassett, E. A., Black, B. E., Foltz. D. R. (2011) HJURP is a CENP-A chromatin assembly factor sufficient to form a functional de novo kinetochore. *J Cell Bio*. **194**, 229-243

Bertran-Alamillo, J., Cattan, V., Schoumacher, M., Codony-Servat, J., Gimenez-Capitan, A., Cantero, F., Burbridge, M., Rodriguez, S., Tezido, C., Roman, R., et al. (2019) AURKB as a target in non-small cell lung cancer with acquired resistance to anti-EGFR therapy. *Nat Commun*, **10**, 1812

Borowicz, S., Scoyk, M. V., Avasarala, S., Rathinam, M. K. K., Tauler, J., Bikkavilli, R. K., Winn, R. A. (2014) The soft agar colony formation assay. *J Vis Exp*. **92**, 51998

Boyarchuk, Y., Salic, A., Dasso, M., Arnaoutov, A. (2007) Bub1 is essential for assembly of the functional inner centromere. *J Cell Biol*. **176**, 919-928

Brito, M. B., Goulielmaki, E., Papakonstnti, E. A. (2015) Focus on PTEN regulation. *Front Oncol*, **5**, 166

Brugarolas, J. (2014) Molecular genetics of clear-cell renal cell carcinoma. *J Clin Oncol*. **32**, 1968- 1976

Campbell, S. C., Novick, A. C., Belldegrun, A., Blute, M., Chow, G., Derweesh, I. H., Faraday, M. M., Kaouk, J. H., Leveilee, R. J., Matin, S. F. (2009) Guideline for management of the clinical T1 renal mass. *J Urol*. **184**, 1271-1279

Carcer, G. (2019) The Mitotic Cancer Target Polo-Like Kinase 1: Oncogene or Tumor Suppressor? *Genes (Basel)*. **10**, 208

Chohan, T. A., Qian, H., Pan, Y., Chen, J. Z. (2015) Cyclin-dependent kinase-2 as a target for cancer therapy: progress in the development of CDK2 inhibitors as anti-cancer agents. *Curr Med Chem*, **22**, 237-263

Chow, W., Dong, L., Devesa, S. (2010) Epidemiology and risk factors for kidney cancer. *Nat Rev Urol*, **7**, 245- 257

Chun, H., Chung, K. Kim, H. C., Kang, J., Kang, M., Kim, J., Choi, E., Jung, K., Kim, M., Song, E., Kim, S., Won, M., Lee, H. (2010). OIP5 Is a Highly Expressed Potential Therapeutic Target for Colorectal and Gastric Cancers. *BMB Rep*. **43**, 349-354

Decastro, G. J., McKiernan, J. M. (2008) Renal cell carcinoma: histological classification and correlation with imaging findings. *Urol Clin North Am*. **35**, 581-592

Enserink, J., Kolodner, R. D. (2010) An overview of Cdk1-controlled targets and processes. *Cell Division*, **5**, 1747-1028-5-11

Feitelson, M. A., Arzumanyan, A., Kulathinal, R. J., Blain, S. W., Holcombe, R.F., Mahajna, J., Marino, M., Martinez-Chantar, M. L., Nawroth, R., Sanchez-Garcia, I. (2015) Sustained proliferation in cancer: mechanisms and novel therapeutic targets. *Semin Cancer Biol***. 35**, S25-S54

Fleitz, J. M., Wootton-Gorges, S. L., Wyatt- Ashmead, J., McGavran, L., Koyle, M., West, D. C., Kurzrock, E. A., Martin, K. W., Odom, L. F. (2003) Renal cell carcinoma in long-term survivors of advanced stage neuroblastoma in early childhood. *Pediatr Radiol*, **33**, 540-545

Fouad, Y. A., Aanei, C. (2017) Revisiting the hallmarks of cancer. *Am J Cancer Res*. **7**, 1016-1036

Grandinetti, C. A., Goldspiel, B. R. (2007) Sorafenib and sunitinib: novel targeted therapies for renal cell cancer. *Pharmacotherapy*. **27**, 1125-1144

Gray, R. E., Harris, G. T. (2019) Renal Cell Carcinoma: Diagnosis and Management. *Am Fam Physician*, **99**, 179-184

Gascoigne, K. E., Takeuchi, K., Suzuki, A., Hori, T., Fukagawa, T., Cheeseman, I. M. (2014) Induced ectopic kinetochore assembly bypasses the requirement for CENP-A nucleosomes. *Cell*. **145**, 410-422

Gong, M., Xu, Y., Dong, W., Guo, G., Ni, W., Wang, Y., Wang, Y., An, R. (2013). Expression of Opa interacting protein 5 (OIP5) is associated with tumor stage and prognosis of clear cell renal cell carcinoma. *Acta Histomchem*, **115**, 810-815

Hans, F., Dimitrov, S. (2001) Histone H3 phosphorylation and cell division. *Oncogene*. **20,** 3021-3027

Hatzivassiliou, G., Song, K., Yen, I., Brandhuyber, B., Anderson, D., Alvarado, R., Ludlam, M., Stokoe, D., Gloor, S., Vigers, G., et al. (2003) RAF inhibitors prime wild-type RAF to activate the MAPK pathway and enhance growth. *Nature*. **464**, 431-435

He, J., Zhao, Y., Zhao, E., Wang, X., Dong, Z., Chen, Y., Yang, L., Cui. H. (2018) Cancer -testis specific gene OIP5: a downstream gene of E2F1 that promotes tumorigenesis and metastasis in glioblastoma by stabilizing E2F1 signaling. *Neuro Oncol*. **20**, 1173-1184

Hongo, F., Takaha, N., Oishi, M., Ueda, T., Nakamura, T., Naitoh, Y., Naya, T., Kamoi, K., Okihara, K., Matsuhima, T., et al. (2014) CDK1 and CDK2 activity is a strong predictor of renal cell carcinoma recurrence. *Urol Oncol*, **32**, 1240-1206

Hotte, S, J., Kapoor, A., Basappa, N., Bjarnason,G., Canil, C., Conter, H. J., Czaykowski, G., Graham, J., Gray, S., Heng, D. Y. C. et al. (2019) Management of Advanced Kidney Cancer: Kidney Cancer Research Network of Canada (KCRNC) consensus update 2019. *Can Urol Assoc*, **13**, 343- 354

Hsieh, J. J., Purdue, M. P., Signoretti, S., Swanton, C., Albiges, L., Schmidinger. M., Heng, D. Y., Larkin, J., Ficarra, V. (2017) Renal cell carcinoma. *Nat Rev Dis Primers*. **3**, 17009

Hua, L., Zhang, L., Zhang, X., Cui, Z. (2017) PI3K/AKT/mTOR pathway promotes progestin resistance in endometrial cancer cells by inhibition of autophagy. *Onco Targets Ther*. **10**, 2865-2871

Hyland, E. M., Cosgrove, M. S., Molina, H., Wang, D., Pandey, A.,Cottee, R. J., Boeke, J. D. (2005) Insights into the Role of Histone H3 and Histone H4 Core Modifiable Residues in Saccharomyces cerevisiae. *Mol Cell Biol*, **25**, 10060-10070

Jonasch, E., Gao, Jianjun, Rathmell, W. K. (2014). Renal cell carcinoma. *BMJ*. **349**, g4797

Jung, J. (2014) Human Tumor Xenograft Models for Preclinical Assessment of Anticancer Drug Development. *Toxicol Res*, **30**, 1-5

Justus, C. R., Leffler, N., Ruiz-Echevarria, M. R., Yang, L. V. (2014) In vitro cell migration and invasion assays. *J Vis Exp*. **88**, 51046

Kalra, S., Atkinson, B. J., Matrana, M. R., Matin, S. F., Wood, C. G., Karma, J. A., Tamboli, P., Sircar, K., Rao, P., Corn, P. G., *et al.*. (2016) Prognosis of patients with metastatic renal cell carcinoma and pancreatic metastases. *BJU Int.* **117**, 761-765.

Koinuma, J., Akiyama, H., Fujita, M., Hosokawa, M., Tsuchiya, E., Kondo, S., Nakamura, Y., Daigo, T. (2012) Characterization of an Opa Interacting Protein 5 Involved in Lung and Esophageal Carcinogenesis. *Cancer Sci*. **103**, 577-586

Kovacs, G., Fuzesi, L., E4manual, A., Kung, H. F. (1991) Cytogenetics of papillary renal cell tumors. *Gene Chromosomes Cancer*. **3**, 249-255

Li, H., Zhang, J., Lee, M., Yu, G., Han, X., Kim, D. (2017) OIP5, a target of miR-15b-5p, regulates hepatocellular carcinoma growth and metastasis through the AKT/mTORC1 and β-catenin signaling pathways. *Oncotarget*. **8**, 18129- 18144

Li, L., Zhao, G. D., Shi, Z., Qi, L., Zhou, L., Fu, Z. (2016) The Ras/Raf/MEK/ERK signaling pathway and its role in the occurrence and development of HCC. *Oncol Lett*, **12**, 3045-3050

Li, Y., Xiao, F., Li, W., Hu, P., Xu, R., Li, G., Zhu, C. (2019) Overexpression of Opa interacting protein 5 increases the progression of liver cancer via BMPR2/JUN/CHEK1/RAC1 dysregulation. *Oncol Rep*, **41**, 2075-2088

Linehan, W. M., Spellman, P. T., Ricketts, C. J., Creighton, C. J., Fei, S. S., Davis, C., Wheeler, D. A., Murray, A., Schmidt, L. S., Vocke, C. D et al. (2015) Comprehensive Molecular Characterization of Papillary Renal-Cell Carcinoma. *N Eng J Med*. **375**, 135-145

Liu, Z., Ren, J., Cao, J., He, J., Yao, X., Jin, C., Xue, Y. (2013) Systematic analysis of the Plk-mediated phosphoregulation in eukaryotes. *Briefing in Bioinformatics*, **14**, 344-360

Liu, Z., Sun, Q., Wang, X (2017) PLK1, A Potential Target for Cancer Therapy. *Transl Oncol*, **10**, 22-32

Lopez-Beltran, A., Carrasco, J. C., Cheng, L., Scarpelli, M., Kirkali, Z., Montironi, R.

(2009) 2009 update on the classification of renal epithelial tumors in adults. *Int J Urol*, **16**, 432-443

Manning, B. D., Cantley, L. C. (2009) AKT/PKB Signaling: Navigating Downstream. *Cell*. **129**, 1261-1274

Marencak, J., Ondrusova, N., Ondrus, D. 2017 Recent overview of kidney cancer diagnostics and treatment. *Klin Onkol*. **30**, 175-181s

Maxwell, P. H., Wiesener, M. S., Chang, G. W., Clifford, S. C., Vaux, E. C., Cockman, M. E., Whykoff, C. C., Pugh, C. W., Maher, E. R., Ratcliffe, P. J. (1999) The tumour suppressor protein VHL targets hypoxia-inducible factors for oxygen-dependent proteolysis. *Nature.* **399**, 271-275

McMubery, J. A., Steelman, L. S., Chappell, W. H., Abrams, S. L., Wong, E. W., Chang, D., Lehmann, B., Terrian, D. M., Milella, M., Tafuri, A., et al. (2007) Roles of the Raf/MEK/ERK pathway in cell growth, malignant transformation. *BioChim Biophys Acta*, **1773**, 1262-1284

Medina-Rico, M., Ramos, H. L., Lobo, M., Romo, J., Prada, J. G. (2018) Epidemiology of renal cancer in developing countries: Review of the literature. *Can Urol Asoc J.* **12**, E154-E162

Muglia, V. F., Prando, A. (2015) Renal cell carcinoma: histological classification and correlation with imaging findings. *Radiol Bras*, **48**, 166-174

Nabi, S, Kessler, E. R., Bernard, B., Flaig, T. W., Lam, E. T. (2018) Renal cell carcinoma: a review of biology and pathophysiology. *F1000Res*. **7**, 307-317

McCrubrey, J. A., Steelman, L. S., Chappel, W. H., Abrams, S. L., Wong, E. W. T., Lehmann, B., Trrian, D. M., Milella, M., Tafuri, A., Sticala, F. (2007). Roles of the Raf/MEK/ERK pathway in cell growth, malignant transformation and drug resistance. *Biochim Biophys Acta*, **1773**, 1263-1284

McKinley, K. L., Cheeseman, I. M. (2015) Polo-like kinase 1 licenses CENP-A deposition at centromeres. *Cell*, **158**, 397-411

Nerli, R.B., Pattanshetti, S., Ghagane, S.C., Malur, P.R. (2015) Chromophobe renal cell carcinoma: Comprehensive analysis of 11 cases. *Clin Cancer Investig J*. **4**, 9-12

Nordi, I. K., Zasadzinska, E., Stellfox, M. E., Knippler, C. M., Foltz, D. R. (2016) Licensing of Centromeric Chromatin Assembly through the Mis18α-Mis18β Heterotetramer. *Mol Cell*, **61**, 774-787

van Oostenbrugge, T. J., Futterer, J. J., Mulders, P. F. A. (2018) Diagnostic Imaging for Solid Renal Tumors: A Pictorial Review. *Kidney Cancer*, **2**, 79- 83

Pan, D., Walstein, K., Take, A., Bier, S., Kaiser, N., Musacchio, A. (2019). Mechanism of centromere recruitment of the CENP-A chaperone HJURP and its implications for centromere licensing. *Nat Commun*, **10**, 4046

Peng, C., Zeng, Q., Su, J., Kuang, Y., He, Y., Zhao, S., Zhang, J., Ma, W., Bode, A., Dong, Z., Chen, X. (2016) Cyclin dependent kinase 2 (CDK2) is a key mediator for

EGF-induced cell transformation mediated through the ELK4/c-Fos signaling pathway. *Oncogene*, **35**, 1170-1179

Prevo, R., Pirovano, G., Puliyadi, R., Herbert, K. J., Rodrigeuz-Berriguete, G., Docherty, A., Greaves, W., McKenna, W. G., Higgins, G. (2018) CDK1 inhibition sensitizes normal cells to DNA damage in a cell cycle dependent manner. *Cell Cycle*. **17**, 1513-1523s

Qian, C., Mei, Y., Zhang, J. (2017) Cancer metastasis: issue and challenges. *Chin J Cancer*. **36**, 38

Rafehi, H., Orlowski, C., Georgiadis, G. T., Ververis, K., El-Osta, A., Karagiannis, T. C. (2011) Cologoenic assay: Adherent Cells. *J Vis Exp*. **49**, 2573

Rathmell, K. W., Chen, F., Creighton, C. J. (2015) Genomics of chromophobe renal cell carcinoma: implications from a rare tumor for pan-cancer studies. *Oncoscience*. **2**, 81-90

Regnier, V., Vagnarelli, P., Fukagawa, T., Zerjal, T., Burns, E., Trouche, D., Earnshaw, W., Brown, W. (2005) CENP-A Is Required for Accurate Chromosome Segregation and Sustained Kinetochore Association of BubR1. *Mol Cell Biol*. **25**, 3967-3981

Ricke, R. M., Jeganathan, K. B., van Deursen, J. M (2011) Bub1 overexpression induces aneuploidy and tumor formation through Aurora B kinase hyperactivation. *J Cell Bio*. **193**, 1049-1064

Sanchez-Gastaldo, A., Kempf., E., Alba, A. G., Duran, I. (2017) Systemic treatment of renal cell cancer: A comprehensive review. *Can Treat Rev*. **60**, 77-89

Scholzen, T., Gerdes, J. (2000) The Ki-67 protein: from the known and the unknown. J *Cell Physiol*. **182**, 311-322

Schubbar, E., Kovacs, A., Hajizadeh, S., Parris, T. Z., Nemes, S., Gunnarsdottir, K., Einbeigi, Z., Karlsson, P., Helou, K. (2013) Elevated cyclin B2 expression in invasive breast carcinoma is associated with unfavorable clinical outcome. *BMC Cancer*, **13**, 1471-2407-13-1

Schmucker, S., Sumara, I. (2014) Molecular dynamics of PLK1 during mitosis. *Mol Cell Oncol.* **1**, e954507

Shultz, L. D., Goodwin, N., Ishikawa, F., Hosur, V., Lyons, B., Greiner, D. L. (2015). Human Cancer Growth and Therapy In NOD/SCID/IL2Rγnull (NSG) Mice. *Cold Spring Harb Protoc*. **2014**, 694-708

Smith, S. L., Bowers, N. L., Betticher, D. C., Gautschi, O., Ratschiller, D., Hoban, P. R., Booton, R., Santibanez, M. F., Heighway, J. (2005) Overexpression of aurora B kinase (AURKB) in primary non-small cell lung carcinoma is frequent, generally driven from one allele, and correlates with the level of genetic instability. *Br J Cancer*. **93**, 719-729

Srigely, J. R., Eble, J. N. (1998) Collecting duct carcinoma of kidney. *Semin Diagn Pathol*. **15,** 54-67

Stellfox, M.E., Nardi, I. K., Knippler, C. M., Foltz, D. R (2016) Differential binding partners of thee Mis18α/β YIPPEE domains regulate Mis18 complex recruitment to centromeres. *Cell Rep*. **15**, 2127- 2135

Sur, S., Agrawal, D (2016) Phosphatases and Kinases Regulating CDC25 Activity in the Cell Cycle: Clinical Implications of CDC25 Overexpression and Potential Treatment Strategies. *Mol Cell Biochem*, **416**, 33-46

Takeshi H., Yohta, F., Osamu, I., Yoh, A., Kohta, T., Misuhiro, Y. (2004) Mis16 and Mis18 Are Required for CENP-A Loading and Histone Deacetylation at Centromeres. *Cell*. **118**, 715- 729

Tan, H., Norton, E., Ye, Z., Hafez, K., Gore, J., Miller, D. C. (2013) Long-term survival following partial versus radical nephrectomy among older patients with early-stage kidney cancer. *JAMA*, **307**, 10.1001

Tasesse, S., Caldon, E. C., Tilelly, W., Wang, S. (2019) Cyclinn-dependent kinase 2 inhibitors in cancer therapy: An update. *J. Med. Chem.* **62**, 4233-4251

Toyoshima-Morimoto, F., Taniguchi, E., Nishida, E. (2002) Plk1 promotes nuclear translocation of human Cdc25C during prophase. *EMBO Rep*, **3**, 341-348

Valdivia, M., Hamdouch, K., Ortiz, M., Astola, A. (2009) CENPA a Genomic Marker for Centromere Activity and Human Diseases. *Curr Genomics*. **10**, 326-335s

Vleugel, M., Hoek, T. A., Tromer, E., Sliedrecht, T., Groenewold, V., Omerzu, M., Kops, G. J. P. (2015) Dissecting the roles of human BUB1 in the spindle assembly checkpoint. *J Cell Sci*, **128**, 2975-2782

Wang, D., Chen, Z., Lin, F., Wang, Z., Gao, Q., Xie, H., Xiao, H., Zhou, Y., Zhang, F., Ma, Y., et al. (2018) OIP5 Promotes Growth, Metastasis and Chemoresistance to Cisplatin in Bladder Cancer Cells. *J Cancer*, **9**, 4684- 4692

Yim, H. (2013) Current clinical trials with polo-like kinase 1 inhibitors in solid tumors. *Anticancer Drugs*, **24**, 999-1006

Yuryev, A., Wennogle, L. (2003). Novel raf kinase protein–protein interactions found by an exhaustive yeast two-hybrid analysis. *Genomics*. **81**, 112-125

Zhang, B., Duan, Z., Zhao, Y. (2009) Mouse models with human immunity and their application in biomedical research. *J Cell Mol Med*, **13**, 1043-1058